A comprehensive search for "anomalies" from neutrino and anti-neutrino oscillations at large mass differences ($\Delta m^2 \approx 1eV^2$) with two LAr–TPC imaging detectors at different distances from the CERN-PS.

October 14th, 2011

M.Antonello, N.Canci, C.Rubbia, E.Segreto, D.Stefan, C.Vignoli
LNGS - INFN, Assergi (AQ), Italy
D. Bagliani, M. De Gerone, S. Dussoni, F. Gatti, G. Testera
Dipartimento di Fisica e INFN, Genova Italy
E.Scantamburlo
Dipartimento di Fisica, University of L'Aquila, Italy
B.Baibussinov, S.Centro, D.Dequal, C.Farnese, A.Fava, D.Gibin, A.Guglielmi, G.Meng, F.Pietropaolo, F.Varanini, S.Ventura
Dipartimento di Fisica e INFN, Università di Padova, Padova, Italy
F.Boffelli, E.Calligarich, R.Dolfini, A.Gigli Berzolari, A.Menegolli, C.Montanari, A.Rappoldi, G.L.Raselli, M.Rossella, A.Zani
Dipartimento di Fisica Nucleare e Teorica e INFN, Università di Pavia, Pavia, Italy
F.Perfetto, A.G.Cocco, G.Fiorillo
Dipartimento di Scienze Fisiche, INFN e Università Federico II, Napoli, Italy
A.Cesana, P.Sala, A.Scaramelli, M.Terrani
INFN, Sezione di Milano e Politecnico, Milano, Italy
M. Bonesini, G. Lucchini
Dipartimento di Fisica, INFN e Università di Milano Bicocca, Milano, Italy
H.Bilokon, G.Mannocchi, L.Periale, P.Picchi, G.Trinchero
Laboratori Nazionali di Frascati (INFN), Frascati, Italy
F.Sergiampietri
INFN, Sezione di Pisa, Pisa, Italy and Department of Physics and Astronomy, University of California, Los Angeles, USA
K.Cieslik, M.Haranczyk
The Henryk Niewodniczanski Institute of Nuclear Physics, Polish Academy of Science, Kraków, Poland
J.Holeczek, J.Kisiel, I.Kochanek, S.Mania
Institute of Physics, University of Silesia, Katowice, Poland
J.Łagoda, T.J.Palczewski, J.Stepaniak, R.Sulej
National Center for Nuclear Research, Warszawa, Poland
P.Płoński, K.Zaremba
Institute for Radioelectronics, Warsaw University of Technology, Warsaw, Poland
D.B.Cline, S.Otwinowski, H.G.Wang, X.Yang
Department of Physics and Astronomy, University of California, Los Angeles, USA
A. Dermenev, S. Gninenko, F. Guber, A. Ivashkin, M. Kirsanov, A. Kurepin, V. Matveev, O. Suvorova, D Tlisov
INR-RAS, Moscow, Russia
A.Ferrari
CERN, Geneva, Switzerland
G.T.Garvey, G.B.Mills, W.C.Louis, R.G.Van de Water
Los Alamos National Laboratory, New Mexico, USA

CERN-SPSC-2011-033 / SPSC-P-345
17/10/2011

ABSTRACT

The present proposal describes an experimental search of sterile neutrinos beyond the Standard Model with the CERN-PS beam and the innovative technology of imaging in ultra-pure cryogenic liquid Argon. The core of the experiment will be the now operational ICARUS T600, the largest LAr-TPC ever built, with a size of about 600 t of imaging mass. The detection method is based on the drift of free electrons over a maximum of 1.5 m. Charge recording as a function of the time allows observing the "image" of the track with a spatial resolution of the order of 3 x 3 x 1 mm^3. The electro-negative impurities currently with the T600 correspond to an equivalent Oxygen content of the order of several tens of ppt (parts per trillion). The LAr-TPC is also an excellent calorimeter and momentum of traversing muons is measured by multiple scattering.

The proposal is based on two strictly identical LAr-TPC detectors observing the electron-neutrino signal in the "Far" and "Near" positions, the first one of about 600 tons placed 850 m the second one of about 150 tons at about 6.5 times shorter distance from the proton target. This project will exploit the ICARUS T600 — now running in the underground experiment CNGS2 with neutrinos from the CERN-SPS — moved from GranSasso to the CERN "Far" position. An additional ($\frac{1}{4}$) of the T600 detector (T150) will be constructed and located in the "Near" position.

In the two positions, the radial and energy spectra of the ν_e beam are practically identical. Comparing the two detectors, in absence of oscillations, all cross sections and experimental biases cancel out and the two experimentally observed event distributions must be identical. Any difference of the event distributions at the locations of the two detectors might be attributed to the possible existence of ν-oscillations, presumably due to additional neutrinos with a mixing angle $\sin^2 2\theta_{new}$ and a larger mass difference $\left|\Delta m^2_{new}\right|$.

The superior quality of the LAr imaging TPC, now widely experimentally demonstrated, and in particular its unique electron – π^0 discrimination allows full rejection of backgrounds and offers a lossless ν_e detection capability.

Two main anomalies will be explored with both neutrino and anti-neutrino focused beams. According to the first anomaly some of the ν_e ($\bar{\nu}_e$) and/or of the ν_μ ($\bar{\nu}_\mu$) events might be converted into invisible components, leading to observation of oscillatory, distance dependent disappearance rates. In a second anomaly (following LSND and MiniBooNE observations) some distance dependent $\nu_\mu \rightarrow \nu_e$ oscillations may be observed as a ν_e excess, especially in the antineutrino channel.

A total LAr mass of 760 + 200 ton and a reasonable utilization of the CERN-PS with the refurbished TT7 beam line will offer remarkable discovery potentialities, collecting a very large number of unbiased events both in the neutrino and antineutrino channels, largely adequate to definitely settle the origin of the many indications behind the ν-related anomalies.

Table of contents.

1 Introduction

Neutrino oscillations have generally established a coherent picture consistent with the mixing of three physical neutrino ν_e, ν_μ and ν_τ with three mass eigenstates and with small mass differences, $\left|\Delta m^2_{32}\right| \sim 2.4\ 10^{-3}$ eV^2 and $\left|\Delta m^2_{12}\right| \sim 8\ 10^{-5}$ eV^2 [1]. The experimentally measured weak coupling strengths are only poorly known, leaving lots of room for alternatives. The sum of the coupling strengths of different neutrinos is found experimentally very close to three. But it is only assuming that neutrinos, in similarity to charged leptons, have unitary strengths that we may conclude that the resulting number of neutrino kinds is indeed equal to three.

There are a number of *"anomalies"* which, if experimentally confirmed, could be hinting at the presence of additional, larger squared mass differences in the framework of neutrinos with mixing or of other effects. The possible presence of some additional "sterile" neutrinos of less than unitary strength was originally proposed by B. Pontecorvo [2] and it has been discussed since a very long time.

Two distinct classes of "anomalies" pointing at additional Physics beyond the Standard Model in the neutrino sector have been reported, namely a) the apparent reduction in the ν_e low energy neutrinos from nuclear reactors [3] and from the signal from Mega-Curie sources in the Gallium experiments [4, 5] originally designed to detect solar neutrino deficit, and b) evidence for an electron excess signal in interactions coming from neutrinos from particle accelerators [6, 7, 8]. The class a) of phenomena hints at a significant fast disappearance rate in the initial ν_e production and the class b) predicts an anomalous $\nu_\mu \rightarrow \nu_e$ oscillation with similar, large $\left|\Delta m^2_{new}\right|$ values, much greater than the ones of the current three-neutrino mixing model. These experiments may all point out the possible existence of at least one fourth non standard neutrino state, driving neutrino oscillations at a small distance, with typically $\left|\Delta m^2_{new}\right| \geq 1$ eV^2 [9]. The existence of one or more additional neutrino states may be also hinted or at least not excluded by cosmological data mainly coming from WMAP and other observations [10].

It is only because the masses of known neutrino species are so small, that their contribution to the Dark Matter of the Universe can be excluded. The presence of massive sterile neutrinos may also contribute to clarify the Dark Matter problem.

A new experiment at CERN PS beam is hereby proposed in order to definitely clarify the existence of such "anomalies" in the above mentioned parameter range. It is based on two strictly identical LAr-TPC detectors [11] observing the electron-neutrino signal in the Far and Near positions from the proton target, the first one of about 600 tons of LAr placed 850 m away and the second of about 150 tons at a ~ 6.5 times smaller distance [12]. In absence

of oscillations the two experimentally observed event distributions must be identical, the background electron neutrino radial and energy distributions being extremely similar in the two positions. All cross sections and experimental biases cancel out. Any difference in the event distributions between the two detectors should therefore be attributed to the existence of oscillations. Both the mixing angle $\sin^2 2\theta_{new}$ and the mass difference $\left|\Delta m^2_{new}\right|$ can then be separately measured.

Some of the relevant above mentioned neutrino "anomalies" that will be addressed by the proposed experiment hint at the possibility of a common origin, due to new physics beyond the present three-neutrino model.

1.1 The SAGE and Gallex experiments

In the nineties, SAGE [4] and GALLEX [5] experiments, designed to determine solar neutrino flux, also recorded the ν_e calibration signal produced by intense artificial k-capture sources of ^{51}Cr and ^{37}Ar placed at very short distance from the detector. The averaged result of the ratio R between the source detected and produced neutrino rates are consistent with each other, R = 0.86 ± 0.05 but about 2.7 standard deviations away from the R = 1 expectation. The result is somewhat influenced by uncertainties in the nuclear models, which however may not be enough to bring R to unity [13]. Best-fit values may favour the existence of an undetected sterile neutrino with a 2.3 σ evidence in a broad range of values centred around $\left|\Delta m^2_{new}\right| \simeq 2$ eV^2 and $\sin^2 2\theta_{new} \simeq 0.3$ [9].

1.2 The reactor anti-neutrino experiments

Recently a re-evaluation of all the reactor anti-neutrino spectra has increased the flux by about 3% [3]. With such a new flux evaluation, the ratio between the observed and predicted rates is decreased to R = 0.937 ± 0.027, leading to a deviation of 2.3 σ from unity (98.4 % confidence level) (Figure 1). However, present reactor experiments explore oscillation regions far from $\left|\Delta m^2_{new}\right|$, with the only exception of the ILL experiment (at 9 m), which unfortunately had a very modest statistical impact (68 % confidence level). Assuming for instance $\left|\Delta m^2_{new}\right| = 2.0$ eV^2 and $E_\nu = 2$ MeV the first minimum of $R = 1 - \sin^2 2\theta_{new} \sin^2(1.27\ \Delta m^2_{new}[eV^2]\ L[m]/E_\nu[MeV])$ occurs at L = 1.24 m and the full pattern repeats each L = 2.47 m. The actual oscillatory pattern may be significantly washed out by the dimension of the reactor core and by the energy resolution of the detector and a reasonably short flight-path distance from the reactor core is necessary.

1.3 The LSND and MiniBooNE experiments

The MiniBooNE experiment [7] used a horn focused neutrino beam from 8 GeV protons of the FNAL Booster to verify the anomaly observed by

the previous LNSD experiment [6] in which $\nu_e + p \rightarrow e^+ + n$ interactions in excess of the expected contributions due to $\bar{\nu}_e$ production have been detected.

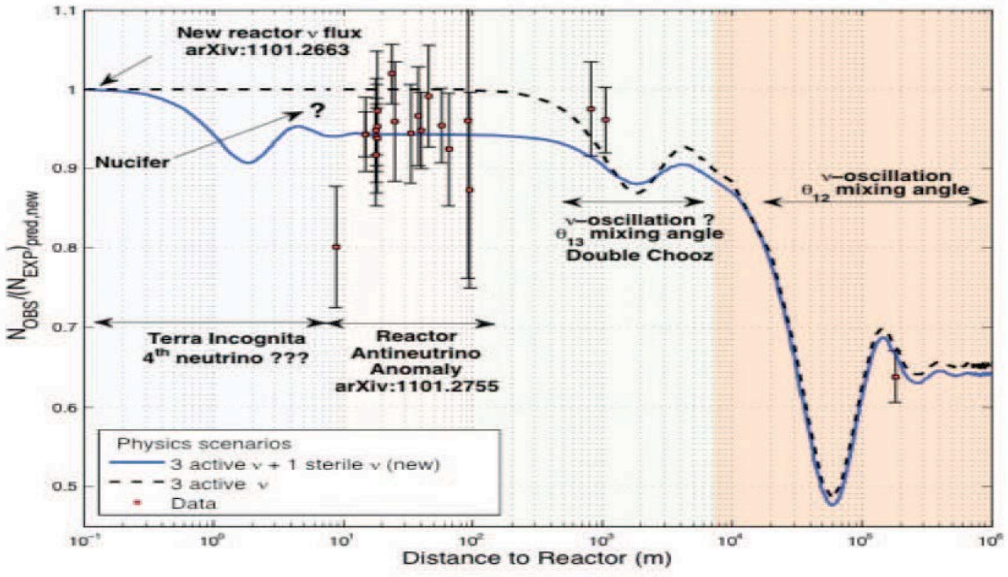

Figure 1. Experimental results at nuclear reactors, compared to antineutrino flux predictions taking into account the new spectra calculations. Fits are performed in two different scenarios, including also the presence of a sterile neutrino component [3].

The anomalous LSND signal (87.9 ± 22.4 ± 6.0) represented a 3.8 σ effect for L/E distances of about 0.5 ÷ 1.0 m/MeV. As well known, explaining this LNSD signal with neutrino oscillations would imply an additional mass-squared difference largely in excess of the standard three-neutrino oscillation values. The 450 ton liquid scintillator of MiniBooNe detector was exposed at a 0.7 GeV neutrino beam at 550 m from the target with an integrated intensity of 6.6 x 10^{20} pot. While the LSND like anomaly seems to be absent in the neutrino data, a new anomaly appears at much smaller values of the neutrino energy.

The more recent MiniBooNE antineutrino run (8.58 x 10^{20} pot) [8] shows however the direct presence of a LSND like $\bar{\nu}_\mu \rightarrow \bar{\nu}_e$ anomaly for $E_\nu >$ 430 MeV with in addition the event excess at lower energies, in agreement with the peak observed in the neutrino run. The result is compelling with respect to the ordinary two-neutrino fit, indicating a 91.1 % probability for an anomalous excess in $\bar{\nu}_e$ production broadly compatible with the expectation of LNSD experiment, dominant in the antineutrino channel (Figure 2). This anomaly, completely different from the claimed disappearance rate in the $\bar{\nu}_e$ channel, may indicate a more complex physics situation. It may be a not negligible contribution of the type $U_{\mu 4}$ due to additional oscillations in the direct channel $\bar{\nu}_\mu \rightarrow \bar{\nu}_e$ or some other unknown mechanism.

The tension between the neutrino and antineutrino MiniBooNE and LSND data seems to indicate a difference of the effective mixing angles in the neutrino and antineutrino channels. Such a difference, if confirmed for in-

stance by the presently proposed experiment, could be due to some unknown mechanism, or perhaps even to CPT violation.

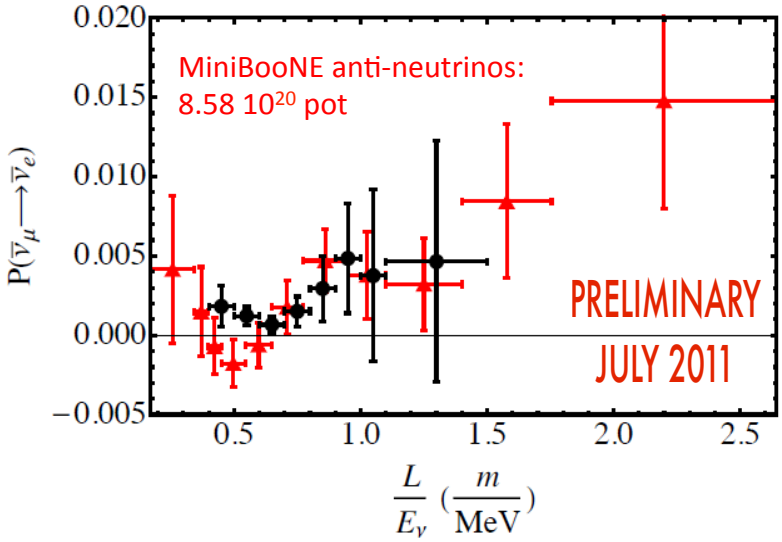

Figure 2. The P($\overline{\nu}_{\mu} \rightarrow \overline{\nu}_{e}$) oscillation probability versus L/Eν as measured by the LSND and MiniBooNE experiments [8].

1.4 A common approach?

The above mentioned experiments may hint at some important new phenomena in the neutrino sector (Figure 3). The allowed regions, reported in the top-right frame, are for a sterile neutrino hypothesis from the combination of reactor neutrino experiments, GALLEX and SAGE calibration sources experiments, MiniBooNE reanalysis according to Ref. [9], and the ILL-energy spectrum distortion [3]. Data are well fitted with the 3 + 1 neutrino hypothesis, while the no-oscillation hypothesis is disfavoured at 99.93 % C.L. The marginal $\Delta\chi^2$ profiles for $|\Delta m^2_{new}|$ and $\sin^2 2\theta_{new}$ (1 d.o.f.) lead to the constraints, $|\Delta m^2_{new}| \sim 1.5$ eV^2 and $\sin^2 2\theta_{new} \sim 0.17 \pm 0.08$ (95% C.L.). The best fit values are $|\Delta m^2_{new}| = 2.35 \pm 0.1$ eV^2 and $\sin^2 2\theta_{new} \sim 0.168 \pm 0.04$ (68% C.L.). The electron neutrino disappearance results and the additional $\nu_{\mu} \rightarrow \nu_{e}$ appearance oscillations are potentially entirely different phenomena. However they may share a common Δm^2_{new} in the region of > 1eV^2. The presence of the two alternate phenomena with different values of $\sin^2(2\theta_{new})$, will hint at the presence of an appropriate fourth neutrino mass matrix $U_{4,k}$ with k = μ and e. If confirmed, such a large mass difference will have an important role in the explanation of the existence of the Dark Mass in the Universe.

The remarkable results of the previous considerations encourage more elaborated experiments to finally determine the possibility of a neutrino anomaly beyond the Standard Model with the direct observation of the necessary oscillatory behaviour. As stressed in Ref. [9] such a clearer experimental proof of the presence of the fourth neutrino becomes mandatory.

Although the most attractive interpretation of excess events observed by LSND and MiniBooNe is based on the conception of a light sterile neutrino, there are additional explanations invoking new physics with a single photon in the final state. They are based on a fact that an electron and a converted photon are undistinguishable in these experiments. For instance interactions of the type, $\nu N \to \nu N \gamma$, where the observable is a single γ, approximately collinear with the incident neutrino direction in the lab frame have been proposed [14]. Alternatively the LSND, KARMEN and MiniBooNE results could all be explained in a consistent way by assuming the existence of a heavy sterile neutrino (ν_h) [15, 16], that can be produced above a given energy threshold. The ν_h is created in ν_μ NC interactions and decays subsequently as $\nu_h \to \nu\gamma$, into a photon and a lighter neutrino.

The PS experiment, based on the LAr-TPC ICARUS technology originally proposed for a wide range of applications, which require precision measurements and particles identification, is perfectly suited to investigate and clarify also these hypotheses.

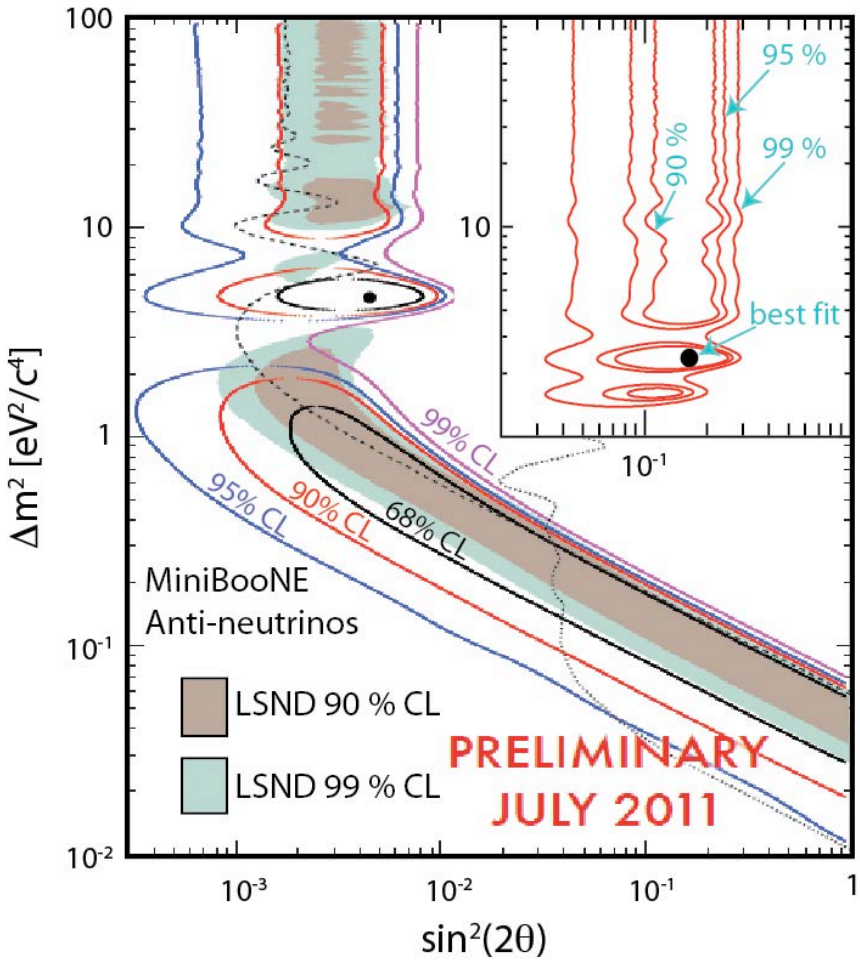

Figure 3. Allowed regions in the oscillation parameter plane for the LSND/MiniBooNE antineutrino anomaly (left) and for the combined results from Ref. [9] for the electron anti-neutrino anomaly in the disappearance rate (top-right).

2 A new approach to neutrino oscillations

In all previously discussed experiments the oscillation pattern of a potential neutrino is not measured directly, the effect being observed at a single distance from the neutrino source. However the direct measurement of a $\sin^2 2\theta_{new}$ oscillation pattern requires necessarily the (simultaneous) observation at different distances in order to separately identify the values of $\left|\Delta m^2_{new}\right|$ and $\sin^2 2\theta_{new}$. The present proposed experiment at the CERN-PS (Figure 4) on the search for spectral differences in electron-like signatures in two identical large mass LAr-TPC detectors in the Far (850 m) and Near (about 150 m) positions away from the source respectively introduces therefore important new features, which should allow a definitive clarification of the previously discussed neutrino anomalies.

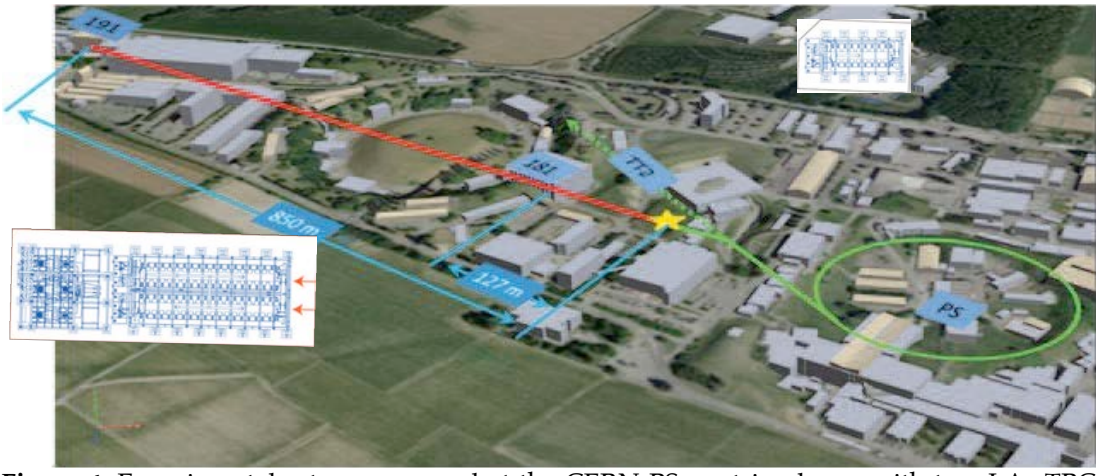

Figure 4. Experimental set-up proposed at the CERN PS neutrino beam with two LAr-TPC detectors.

The proposed experiment will exploit the CERN-PS neutrino beamline, originally used by the BEBC-PS180 Collaboration [17] and successively re-considered by the I216/P311 Collaboration [18]. The neutrino beam will be a low energy ν_μ beam, centred at about 1.5 GeV, produced by 20 GeV protons with expected intensity of 1.25 x 10^{20} pot/yr.

It is a very fortunate circumstance that the CERN-PS ν_e spectra, expected at the level of 0.5 % of ν_μ, are very closely identical in the Near and Far positions (Figure 5). The physical reason of this effect has to be identified in the fact that while the ν_μ spectrum is dominated by the two body $\pi \to \mu\nu_\mu$ decays, where the neutrino directions are narrowly distributed along the axis, the ν_e contamination is dominated by the three body decays of K and μ where there is a much wider neutrino angular spread. The similarity is further enhanced by the fact that the Near and Far detectors have been designed with identical internal configurations, i.e. 3 mm wire pitch and 1.5 m drift length in the TPC's. In absence of oscillations, after some beam related small spatial corrections, the two energy spectra should be a precise copy of each other, independently of the specific experimental event signatures and

without any need of Monte Carlo comparisons. Therefore, an exact observed proportionality between the two ν_e spectra, would imply directly the absence of neutrino oscillations over the measured interval of L/E: any resulting ν_e difference between the two locations, if observed, must be inevitably attributed to the time evolution of the neutrino species.

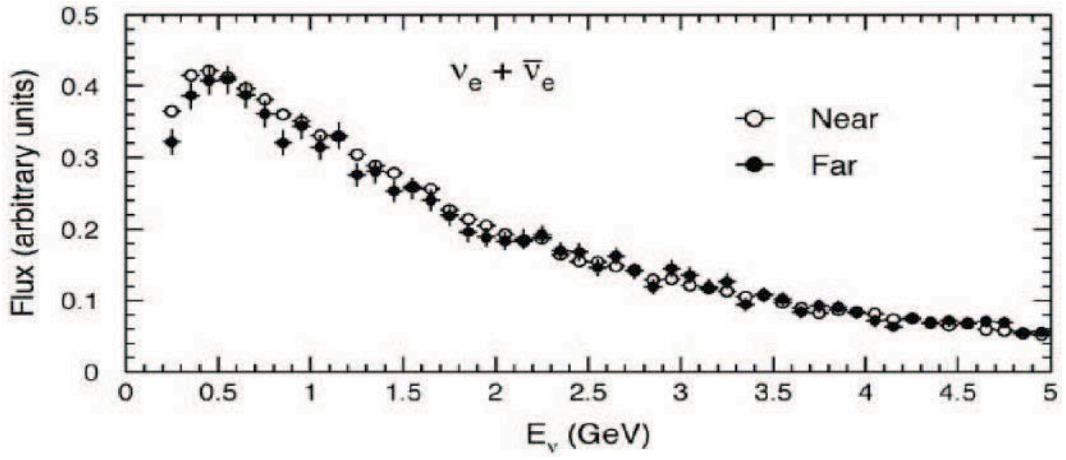

Figure 5. Expected ν_e fluence at Near/Far detector positions as predicted for the I216 proposal.

As an important feature, in the present proposed experiment, both neutrino and anti-neutrino beams will be used. We recall that the LSND claim had been primarily based on anti-neutrino data.

A key issue of the proposed experiment will be the LAr-TPC detection capability of ν_e events in the different channels, thus allowing the reconstruction of the totality of neutrino events, with a very high level rejection of the associated background events, in primis from the π^0 decay. As described in more detail further on, the LAr-TPC technique appears very well suited for this purpose, because of its excellent imaging and calorimetric capabilities, which allow very efficient electron - π^0 separation, together with unambiguous electron identification.

According to the present proposal the ICARUS T600 detector (Figure 6) [11] will be moved from the LNGS laboratory into the Far position of the CERN-PS neutrino beam (Hall B-191) after the completion of the presently running CNGS2 experiment at the end of 2012. An additional "clone" of the LAr structure using the same design will be constructed for the Near configuration, at a distance about 6.5 times shorter.

2.1 The CERN-PS neutrino beam

The original PS Neutrino Facility was realized for the PS169, PS181 and BEBC-PS180 $\nu_\mu \rightarrow \nu_e$ experiments in the early 80's. A 19.2 GeV/c proton beam was extracted from the PS via the transfer tunnel TT2, TT1 and TT7 and impinged on an 80 cm long, 6 mm diameter beryllium target. A magnetic horn – designed to focus positive particles of around 2 GeV/c momenta –

was installed downstream of the target; the secondary particles propagated in a decay tunnel of ~ 50 m length, with a cross-section of 3.5 x 2.8 m^2 for the first 25 m and 5.0 x 2.8 m^2 for the remaining 25 m, in order to allow the decay of mesons with larger angular divergence. The tunnel was then terminated by a 4 m long iron hadron stopper and 65 m of earth to absorb the remaining hadrons and most of the muons (Figure 7).

Figure 6. The ICARUS T600 detector installed in Hall B at LNGS.

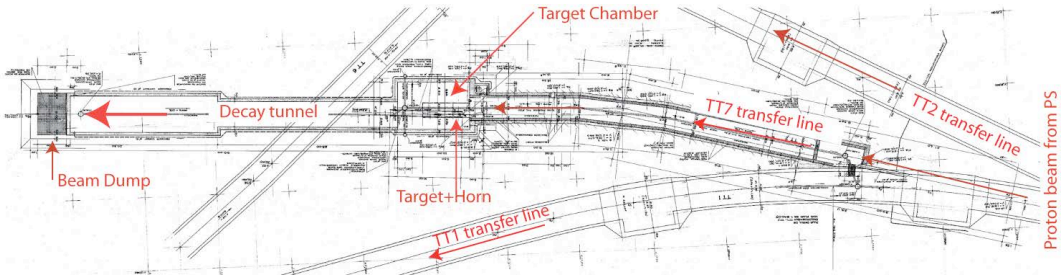

Figure 7. CERN-PS neutrino beam layout.

Preliminary studies about the refurbishing of the PS Neutrino Beam Facility (PSNF) line have been completed at CERN. Large parts of the required infrastructure are already available, but some renovation is needed. The TT7 transfer line, the target chamber and the decay tunnel are in good shape and available for the installation of the proton beam line, target and magnetic horn. Some important elements for the beam refurbishing, such as the main dipoles, quadrupoles, correction dipoles and the transformer for the magnetic horn, can be recuperated, reducing significantly cost and time schedule. For technical details we refer to Ref. [19].

Presently the PS can provide a 20 GeV/c beam of 3 x 10^{13} protons per pulse at a maximum repetition rate of 1.2 s, resulting in about 3.6 x 10^{20} pot/year in 180 days of operation (Table 1) [20]. Assuming a physics run of 200 days and an average machine availability of 85%, a duty cycle of 34% is required to provide 1.25 x 10^{20} pot per physics run on the PSNF target. The concurrent requests for beam availability from the nTOF experiment can be solved by combining the two beams in a single cycle: 7 bunches can be extracted and transferred to the PSNF target and the remaining single bunch can be transferred to the nTOF target (Table 2).

Table 1. Summary of past and present potential PS beam production capabilities for the PSNF

		Old Neutrino Facility		**New Neutrino Facility**	
		PS dedicated Feb-Mar 1983	**PS parallel 1983 - 1984**	**PS dedicated**	**PS parasitic[1)]**
Proton Momentum	[GeV/c]	19.2	19.2	20	20
Protons per pulse	[x10^{13}]	1.2	1.2	3	2.6
Max. rep. rate	[s]	1.2	14.4	1.2	1.2
Beam energy	[kJ]	38	38	96	84
Average Beam Power	[kW]	32	2.5	80[2)]	70[2)]

[1)] The parasitic beam is in the case that the PSNF and nTOF beams will be produce on a single cycle.

[2)] This average beam power is potentially available from the PS provided the losses are within the specified limits and that no other users are present in the PS super cycle.

Table 2. Overview of PSNF dedicated and PSNF/nTOF parasitic primary proton beam time structure

		PSNF		**nTOF[1)]**
		Dedicated	**Parasitic**	
Number of bunches per cycle	-	8	7	1
Total intensity	[x10^{13}]	3	2.63	3.75
Intensity per bunch	[x10^{12}]	3.75	3.75	3.75
Bunch spacing	[ns]	263	263	-
Bunch length	[ns]	~ 65	~ 60	< 25
Burst length	[ns]	2100	1841	-

[1)] Values for nTOF as produced with the PSNF parasitic beam.

Conservative assumptions, based on PS beam scheduling in the last years, show that a sharing of 31.1% of the PS super cycle can be easily obtained. Taking into account also 2 hours/day dedicated to LHC filling, a first estimate gives 0.92 x 10^{20} protons intensity per year. Few weeks of additional dedicated run will be sufficient to fulfill the request of 1.25 x 10^{20} pot/year.

As reference case the neutrino beam set-up used by the BEBC-PS180 experiment has been adopted [17]. An optimized design of new and possibly improved beam optics will be the subject of further studies.

The neutrino beam line geometry has been implemented in the FLUKA Monte Carlo code (a cross section is shown in Figure 8) in collaboration with the CERN EN/STI group [21]. This approach has been successfully adopted in the past also for the CNGS studies, in the framework of a synergic collaboration among the experiments, the engineering and the radioprotection groups [22].

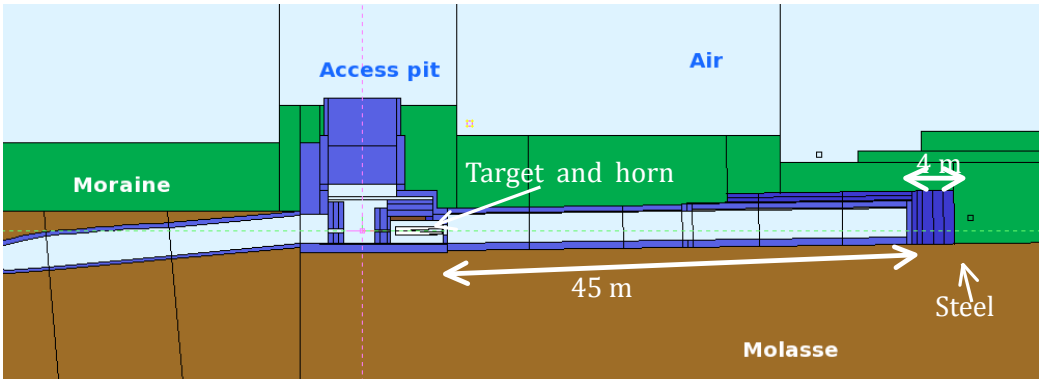

Figure 8: Cross section of the neutrino beam line as implemented in the simulations.

The horn layout is the same as for the PS-180 experiment, namely a ~ 4.5 m log horn pulsed at 120 kA. The target is an 80 cm long graphite cylindrical rod ($\rho = 1.75\ g/cm^3$) of 6 mm diameter, partially inserted within the horn. The assumed proton beam FWHM is of 2 mm. In order to centre the neutrino beam with the proposed location of the far detector, the target/horn assembly has to be rotated horizontally by 19.6 mrad with respect to the axis of the decay tunnel. A vertical inclination of 13.2 mrad with respect to the ground orientation is needed in order to match the direction of the decay tunnel towards the middle of the far detector.

The positively and negatively focussed CERN-PS neutrino spectra are shown respectively in Figure 9-top for the most relevant "Far" position at 850 m from the PS target. Fluxes have been averaged over a 5 m radius at the far position, and over a 2 m radius at the near position, to fit the detector dimensions and the radial shape of the beam. The fluxes calculated by the I216 collaboration and adopted in our previous documents are also shown for comparison. The corresponding $(\nu_e + \bar{\nu}_e)/(\nu_\mu + \bar{\nu}_\mu)$ flux ratio as a function of the incoming neutrino energy is shown in Figure 9-bottom. The flux ratios for negative and positive focussing are similar. As anticipated in the previous sections, the shape of the ν_e spectra, at the far and near locations, are very similar to each other, both for the neutrino and the antineutrino beams (Figure 10). This is a consequence of the wider angular distribution of electron neutrinos coming from the three body decay kinematics of kaons and muons, reflecting in a flat radial distribution at both locations, as shown in Figure 11.

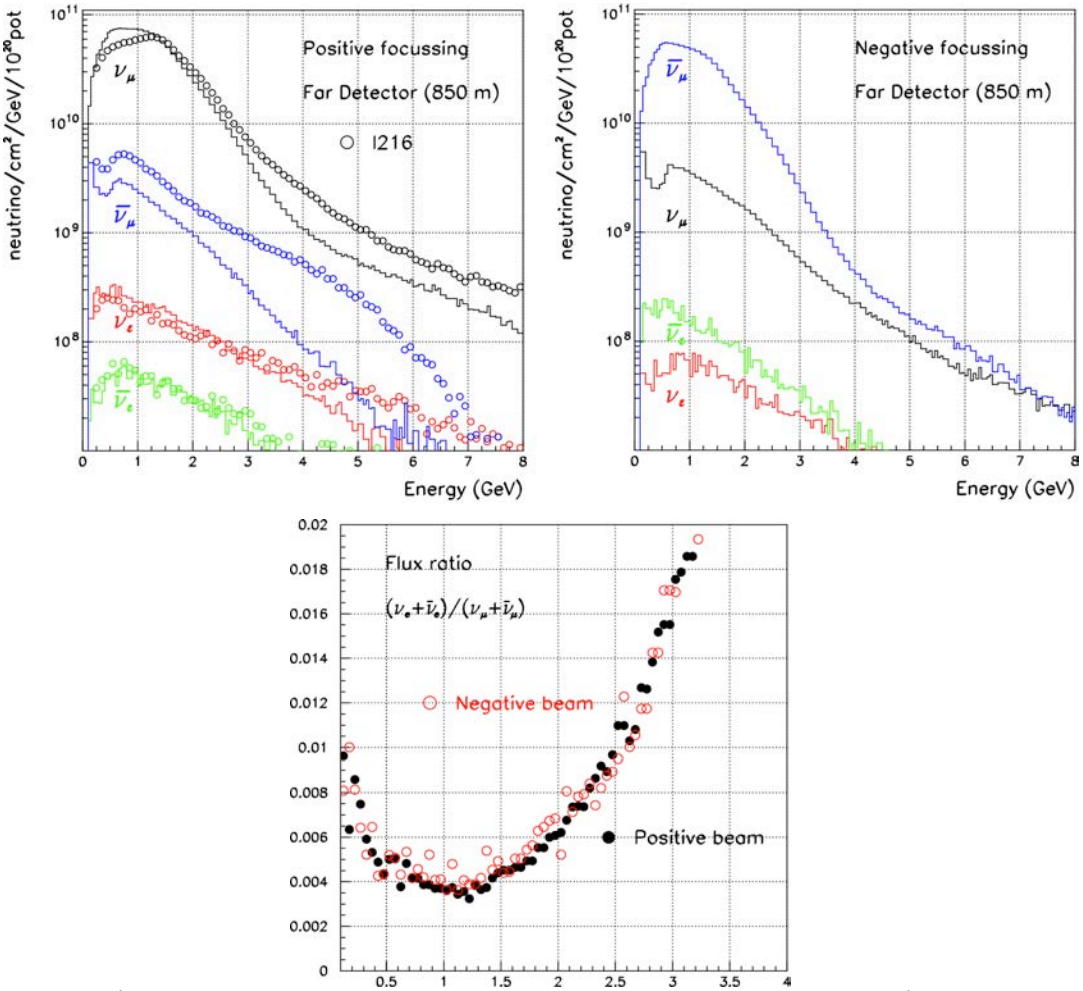

Figure 9 The expected CERN-PS neutrino (top-left) and antineutrino (top-right) beam fluxes in the far position. The corresponding ratios $\left(\nu_e + \bar{\nu}_e\right)/\left(\nu_\mu + \bar{\nu}_\mu\right)$ are also shown (bottom).

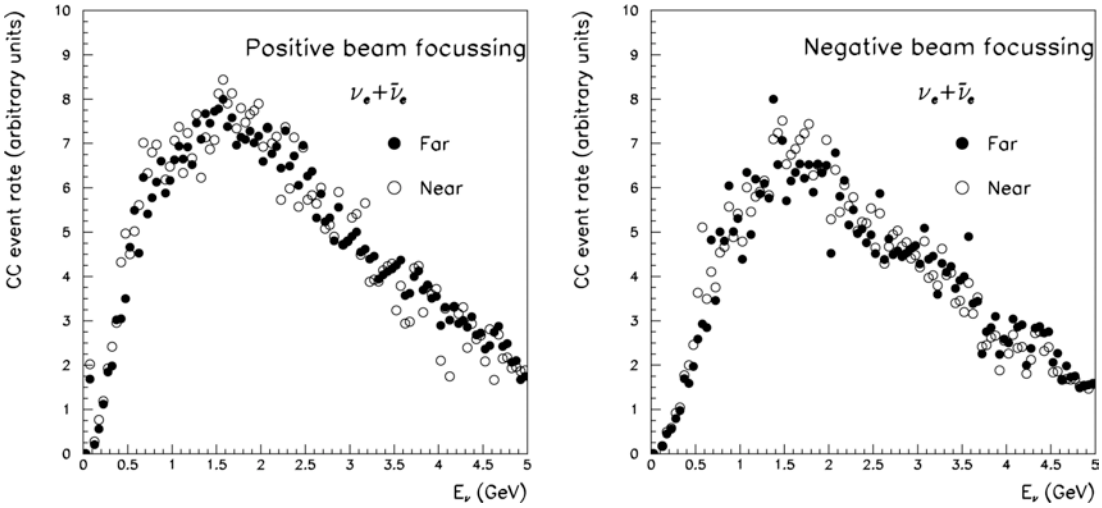

Figure 10. Expected ν_e event rate at Near/Far detector positions in the case of positive (left) and negative (right) focusing.

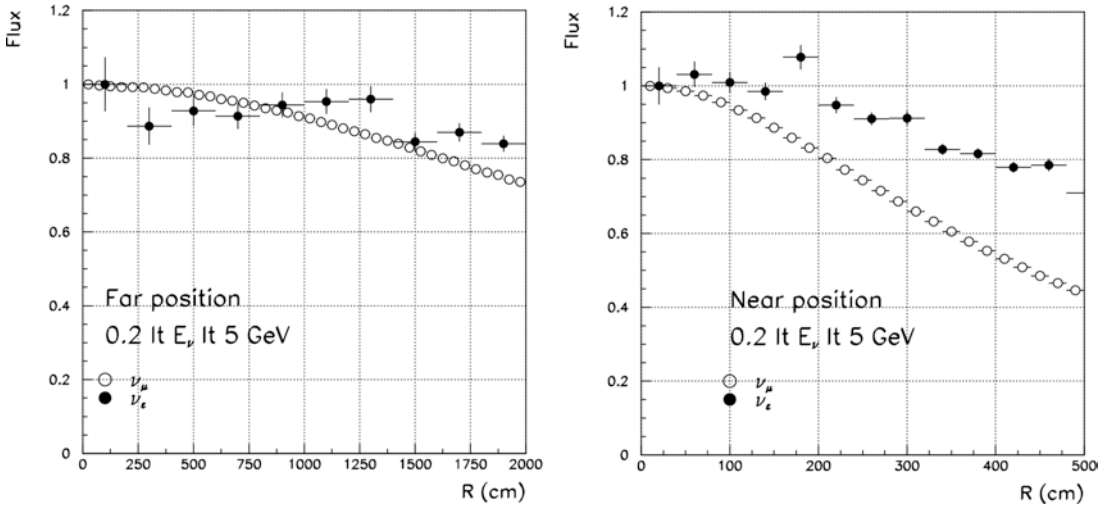

Figure 11. Radial dependence of neutrino fluxes in the energy interval 0.2-5 GeV at the far (left) and near (right) positions.

2.2 A powerful technology: the LAr TPC

Bubble chambers have had a major role in neutrino physics: for instance the well known Gargamelle bubble chamber, in spite of its relative small sensitive mass compared to other electronic calorimetric detectors has contributed in an essential way to the discovery of Neutral Currents and of the Electro Weak components of the Standard Model.

The LAr-TPC technology, first proposed by Carlo Rubbia in 1977 [11], has been developed by the ICARUS group since about two decades [23]. The "bubble chamber like" observation of the neutrino events permits to identify precisely the features of individual events [24]. This is an important difference with respect to all previously reported observations (see for instance LSND and MiniBooNE) which have been based on the more primitive observation of Cerenkov rings produced by PM's at the surface of the detector volume and which are mostly limited to quasi-elastic events.

The technology of the LAr-TPC [25] is conceived as a tool for a completely uniform imaging with high accuracy of massive volumes. The new method of imaging in a noble liquid is based on a truly novel concept of free electron drift as a function of the time, in order to observe the true "image" of the track with an accuracy of the order of 1 mm^3, thus extending to a liquid the idea of the TPC already described for a gas, originally proposed by G. Charpak et al. [26]. The passage from a gas to a liquid is not entirely trivial, since the density is about a factor 1000 larger and therefore a corresponding much higher purity is necessary. The length of the drift of electrons in ultra-pure noble liquid becomes an asset and it must be made as long as possible, up to meters, corresponding to equivalent Oxygen contents of the order of a few tens of ppt (parts per trillion) (Figure 12).

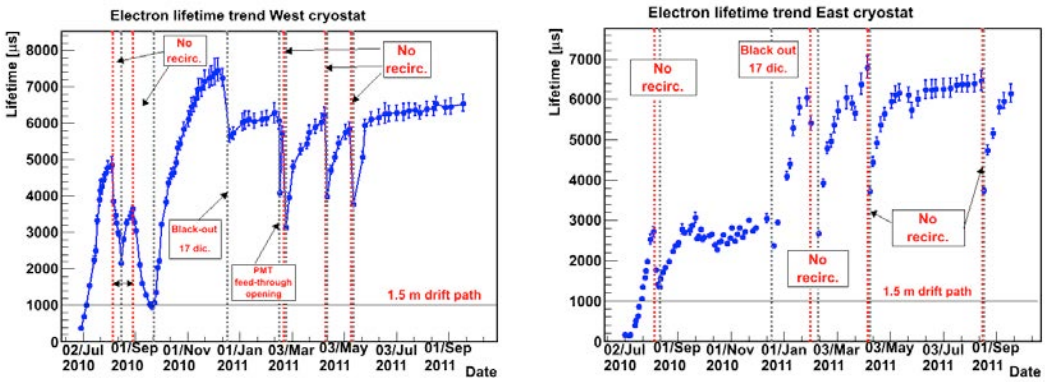

Figure 12. Time evolution of the free electron lifetime in the West (left) and East (right) ICARUS T600 cryostats during the first 15 months of operation at LNGS.

The operational principle of the LAr-TPC is based on the fact that in highly purified LAr ionization tracks can be transported practically undistorted by a uniform electric field over macroscopic distances. Imaging is provided by a suitable set of electrodes (wires) placed at the end of the drift path continuously sensing and recording the signals induced by the drifting electrons. Non-destructive read-out of ionization electrons by charge induction allows detecting the entire signal of electrons crossing subsequent wire planes with different orientation. This provides simultaneously several projective views of the same event, hence allowing space point reconstruction and precise calorimetric measurement (Figure 13).

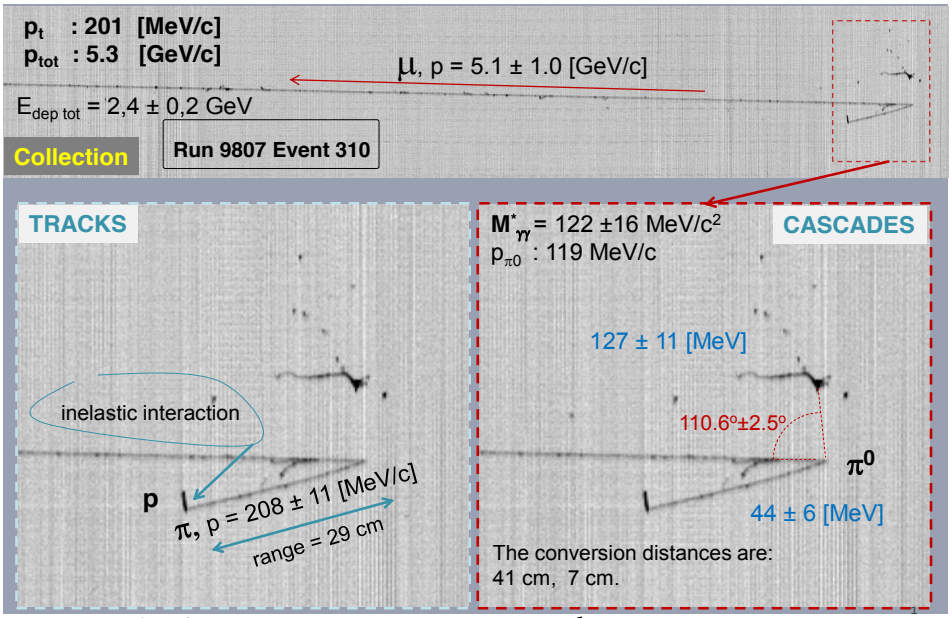

Figure 13. Example of CNGS muon neutrino event in the ICARUS T600 at LNGS. Beside the leading muon spanning the whole detector length, whose momentum is measured by multiple scattering, one charged pion and one π^0 at the interaction vertex are identified and fully reconstructed (visible in the zoomed areas).

2.3 *The T600 detector*

The ICARUS T600 detector [27] presently in operation underground in Hall B of LNGS with the CERN-SPS neutrino beam, is the largest liquid

Argon TPC ever built, with a size of about 760 tons of LAr mass (Figure 14). The design and assembly of the detector relied on industrial support and represents the application of concepts matured in laboratory tests to the kton-scale.

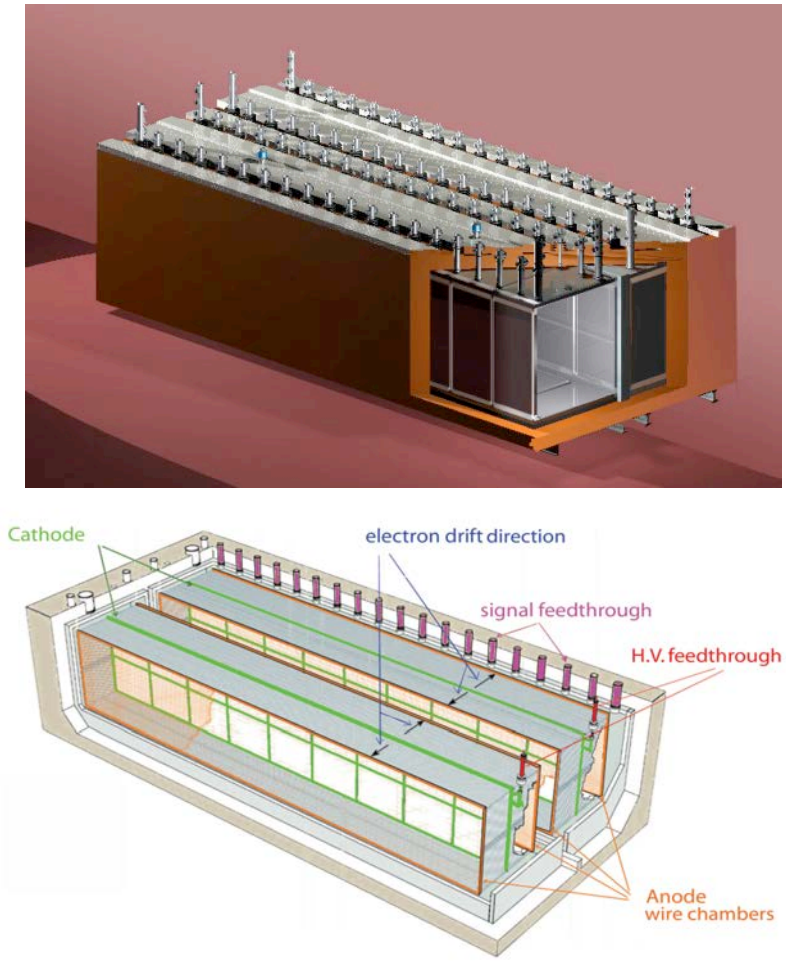

Figure 14. The T600 schematics, showing both half-modules with the inner structures and the common insulation surrounding the detector.

The detector consists of a large cryostat split into two identical, adjacent half-modules (T300), with internal dimensions $3.6 \times 3.9 \times 19.6$ m^3 each, filled with a total of about 760 t of ultra-pure liquid Argon. The active LAr mass is about 476 t.

Each T300 houses two Time Projection Chambers (TPC) separated by a common central cathode, a field shaping system, monitors, probes, and arrays of photo-multiplier tubes (PMTs). Externally the cryostat is surrounded by a set of thermal insulation layers. The detector layout is completed by a cryogenic plant made of a liquid Nitrogen cooling circuit, used to maintain the LAr temperature uniform, and by a system of two LAr purifiers.

Each TPC consists of a system of three vertical parallel planes of wires (17.95 x 3.16 m^2 of surface), 3 mm apart from each other. Wires are made of AISI 304V stainless steel, 150-μm diameter. The first plane faces the drift re-

gion, with horizontal wires, while the other two planes have the wires at ± 60° with respect to the horizontal direction. By appropriate voltage biasing, the first two planes (induction planes) provide signals in non-destructive way, whereas the charge is collected in the last one (collection plane). The maximum drift path, i.e. the distance between the cathode and the wire planes, is 1.5 m and the nominal drift field 500 V/cm. The total number of wires in the T600 detector is about 54,000. The cathode is an array of nine panels of ~ 50% punched stainless-steel sheets. The drift electric field is generated by biasing the central cathode at a negative HV referred to the potential of the first wire plane; the nominal 500 V/cm drift field requires 75 kV on the cathode, provided by a specially designed ultra-high vacuum cryogenic feed-through. The electric field in each drift volume is kept uniform by means of field shaping electrodes, i.e. 29 rectangular rings for each wire chamber. They are set at a potential linearly decreasing from the cathode to the first wire plane through resistive voltage degraders, in steps of 25 MOhm each.

A set of 8 inches ETL-9357-FLA™ PMTs coated with TPB wavelength-shifter is installed inside the cryostats, 20 PMTs in the first half-module and 54 in the second one, just behind the wire chambers. The PMT system is designed to detect the prompt scintillation light for trigger and timing purposes (Figure 15).

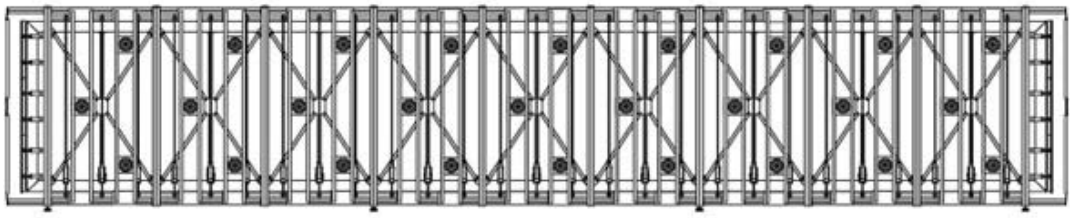

Figure 15. PMT installation layout behind each TPC wire chamber. The distance between PMT's in each row is 2 m. The rows separation is 1 m. In the first T300 module only the middle row is installed.

Each of the two internal detector subsystems is completed by the control instrumentation, i.e. sensors and probes of the slow control system.

The way out of signal cables of the internal detectors and control instrumentation is carried out by means of holes and chimneys located on the ceiling of the two containers. On each T300 cryostat chimneys are aligned (20 per row) in correspondence with the two frames of the wire chambers. Chimneys are terminated with vacuum-tight feed-through flanges allowing the passage of the corresponding wire signal cables (572 per flange) and that of other detector subsystem.

The ICARUS T600 is taking data since May 2010 under optimal and stable conditions, collecting about 10 neutrino and beam related events/day from CNGS together with atmospheric and rare cosmic events. This under-

ground physics campaign will continue until end 2012 at the shut down of the CERN accelerator complex.

2.4 T600 transport from LNGS to CERN

A feasibility study and cost estimate concerning the possible transport of ICARUS T600 from LNGS Hall B to CERN has been performed in close collaboration with the Transport Group of CERN.

Two possible solutions have been studied: 1) transport of the complete T300 cryostats, without the thermal insulation system; 2) transport of the internal detector structures as a common block.

In the first solution, the preferred way out is through the "entrance" of the LNGS TIR gallery to minimize interference with other activities in the Laboratory. However it requires heavy civil engineering works at LNGS, during a relatively long period. 3D computer simulations of the maneuvers have shown that the insertion of the cryostats into the TIR gallery implies some modifications of Hall B such as demolition of existing bumps, reduction of the floor level by 30 cm for ~10 m for the whole hall width, dismantling of OPERA barrack, elimination of lamps and minor equipment around the doors (Figure 16). There are other structures close to the handling volume and accurate verifications are required. Doors and air ducts must be temporarily removed in TIR gallery. Such works are subject to the approval of the LNGS management and should be realized under the LNGS responsibility and supervision.

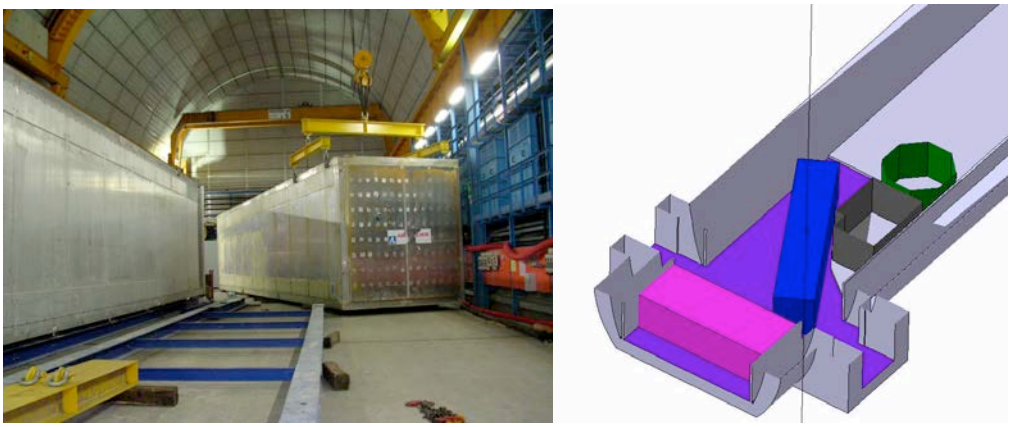

Figure 16. Moving the second T300 module into Hall B at LNGS (left). 3D simulation of the way out; required modification of the hall floor are shown in violet (right).

As an alternative, solution 2 consists in the removal of the internal detectors, whose dimensions (3.9 x 3.6 x 19.8 m^3) are compatible with the maximum movable object size in the present layout of Hall B. Moreover, its overall weight is well under the crane capacity (40 t), which will permit the complete maneuver in hall B with the crane, substantially simplifying the work (Figure 17).

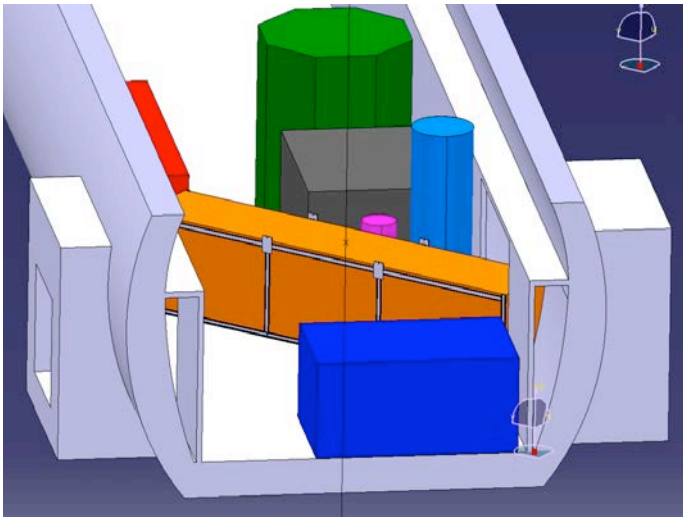

Figure 17. 3D simulation of the way out for a T300 internal detector only (wire chambers, field shaping rings and central cathode.

The internal detector will be extracted fully assembled from cryostats, with an existing, appropriate tooling and introduced in a container and an appropriate clean room will protect and support wire chambers and will be used as interface during transport. This solution permits to avoid major heavy works in Laboratory. In this option, the new cryostats should be built at CERN following the same design of the cryostat of the near detector and the same will be done for the external thermal screen.

2.5 Preparation of the Hall 191 for T600 detector

The old BEBC experimental hall (Bdg. 191) is fully adequate to host the T600 as "Far" detector for the proposed experiment (Figure 18).

The useful surface is about 26 x 45 m^2 and the height is more than 20 m. The clearances of the entrance doors are 16 m in height and 10 m in width. The hall is equipped with two cranes (170 t and 5 t each) placed at about 16 m height spanning the whole surface. Retaining walls around the T600 detector are foreseen to contain potential Argon leaks.

The electrical power distribution and the redundant supply line are already available and provide the 700 kW power required by the whole T600 plant. The main consumption is due to the Stirling cryo-coolers absorbing 45 kW each, to the electronics and DAQ system (150 kW) and to the ancillary cryogenic system such as PLC, valves, instrumentation, pumps, heaters, etc. (200kW).

The existing air ventilation allows evacuating up to 15000 m^3/h in standard operation and 60000 m^3/h in emergency situation, well above the present T600 installation at LNGS. Suction system to evacuate the gas from the bottom of the retaining wall volume has to be installed.

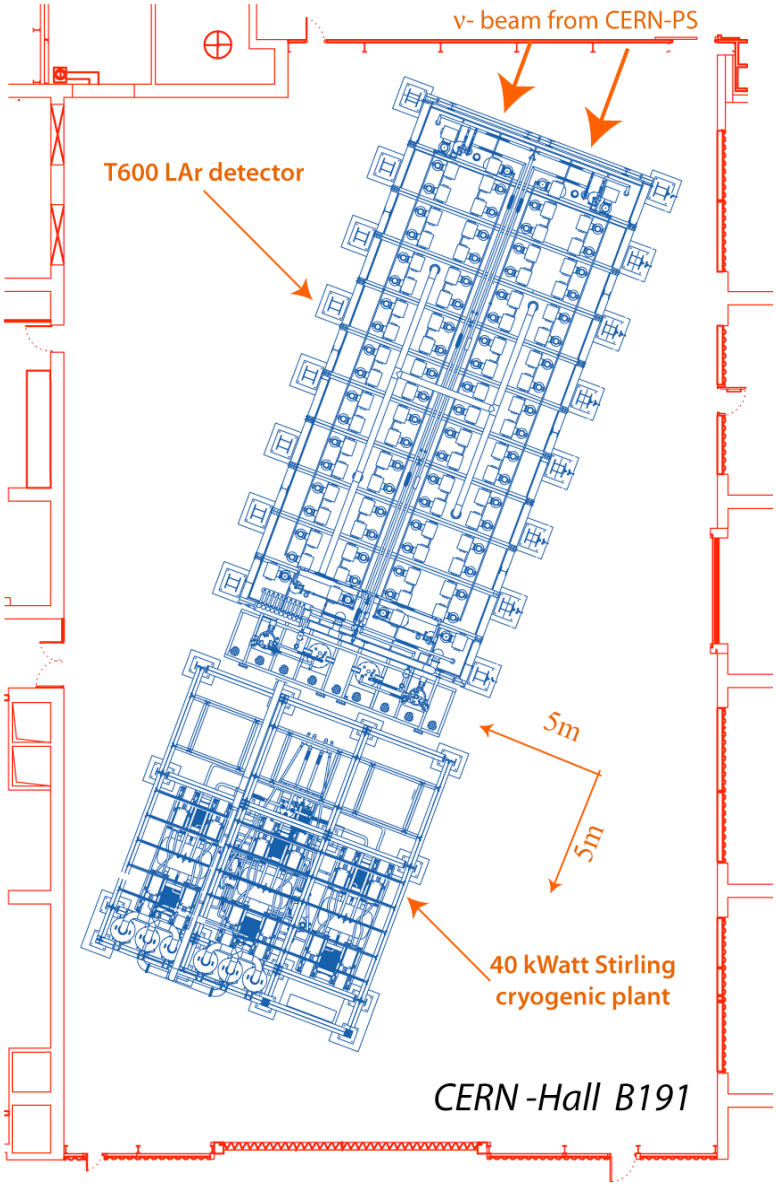

Figure 18. The general layout of the T600 LAr detector in the "Far" Position and of the associated cryogenic equipment in Hall B-191 at CERN. The direction of the neutrino beam is also indicated.

Safety sensors (oxygen deficiency, temperature sensors, smoke sensors, cameras, emergency panels, emergency lights, acoustic alarms, etc.) and PLC control system (PVSS-UNICOS) will be installed as in the LNGS plant.

2.6 T600 installation at CERN

Depending on the adopted transport solution there are two possible scenarios for the T600 re-installation at CERN in Hall 191: (1) re-use of the two T300 half-module cold vessels if they will be integrally transported from LNGS to the BEBC Hall, (2) reconstruction of the two T300 half-module cold vessels if, due to transport difficulties, they will need to be dismounted at LNGS Hall B to extract the wire chambers. In the second option, the new two cold vessels will be rebuilt with the same technique that will be used for the T150 vessel. The collaboration is carefully studying different solutions to op-

timize cost and performance of these cold vessels. Both stainless steel and aluminium solutions are under evaluation taking into account that the new location at CERN will not impose to the mechanical construction and installation the constraints required by underground laboratory such as LNGS. For instance these new vessels do not require to be transportable, so their weight is no longer a key issue.

A key element to realise an adequate and efficient insulation for the two T300 cryostats, is the adoption of thick passive thermal shielding, in particular for the bottom layer in which natural convection motion have to be avoided. This "vacuum free" solution has the advantage of less stringent mechanical constraints and of being intrinsically safe for long term operation.

A possible design could be similar to the one suggested for the ModuLAr proposal, using a platform of Foamglas ($K < 0.049$ W m^{-1} K^{-1} @ room temperature) bricks for the bottom (directly supporting the weight of the 2 T300 half-modules) and perlite filled lateral walls ($K < 0.03$ W m^{-1} K^{-1} @ room temperature) or equivalent materials, adequately fluxed with nitrogen gas. For the top a light insulation solution based on foam or Divinycell™ ($K < 0.025$ W m^{-1} K^{-1} @ room temperature) panels can be adopted (Figure 19).

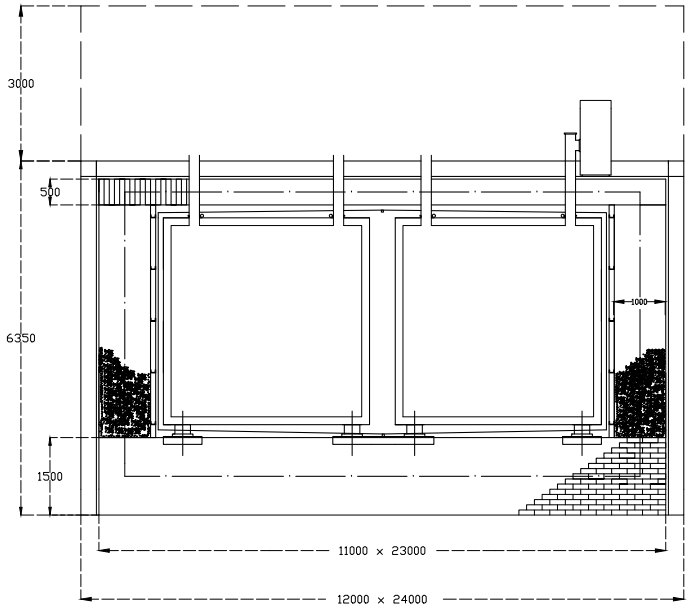

Figure 19. Schematics of a possible solution of a vacuum free insulation for the T600 at CERN.

As first evaluation of the overall heat losses, such a shield can be built with 1.5 m thick bottom (1.5 kW), 1.0 m thick lateral walls (2.4 kW), 0.5 m thick top (2.3 kW), for a total of ~ 6 kW or ~ 7.7 W/m^2 on average. According to the present measurements on the T600 at LNGS, the heat losses through chimneys, cables and pipes, contribute with an additional 4 kW, reaching a total heat input of $Q_{TOT} \approx 10$ kW max.

As in the present T600 design, the residual heat-losses will be compensated by Liquid Nitrogen circulating in thermal screens located between the cold body and the external insulation panels. This will guarantee high LAr temperature uniformity ($\Delta T < 1$ K) throughout the whole LAr volume and thermal gradients regulation during cooling phase ($\Delta T < 50$ K). The Liquid Nitrogen circulates in a closed circuit and the evaporated fraction is condensed back by a battery of Stirling cryo-coolers producing up to 4 kW of cold power each at 90 K. Therefore the global LN_2 consumption of about 225 l/h max will be easily and safely handled a limited number of Stirling cryo-coolers presently installed ad LNGS.

The present design allows the emergency cooling by LN2 gravity circulation both during first cooling and regime phase. It represents a simplification of the circuit without the use of a LN2 circulation pump. This requires LN2 reservoir located at a higher level.

2.7 T150 detector

The design of T150 TPC will be a clone of a single T300 half-module with the length reduced by a factor 2 (about 10 m). This allows exploiting "as it is" the design of the inner detector layout, keeping untouched the wire chamber granularity, the number of wire planes and the 1.5 m maximum drift distance. The cold body (Figure 20), the insulation vessel and the cryogenics equipment will be consistent with the solution adopted for T600 at CERN. The total LAr mass will be 200 t (119 t active mass).

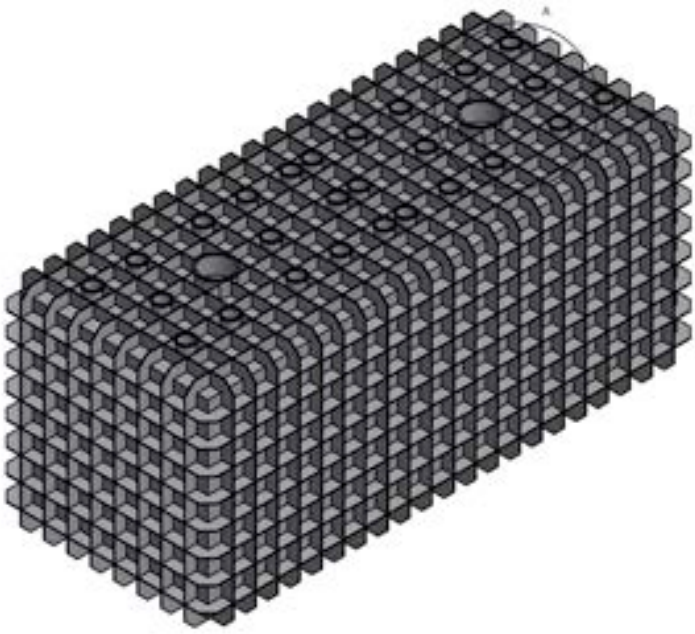

Figure 20. Tentative design of a stainless steel cold vessel for the T150. The execution with AISI 304L will weight approximately 42 t.

The detector dimensions, including passive insulation similar to the one proposed for the "Far" detector, fits perfectly in the already existing pit

of hall B-181 (Figure 21), located at 127 m from PS neutrino beam target and previously used for neutrino oscillation experiments. However, given the present activities in B-181, a second option has been proposed for a new pit in a dedicated building at an indicative location about 10 m upstream of the B-181 pit (see also Figure 22), with a relatively modest variation in the beam rate [28].

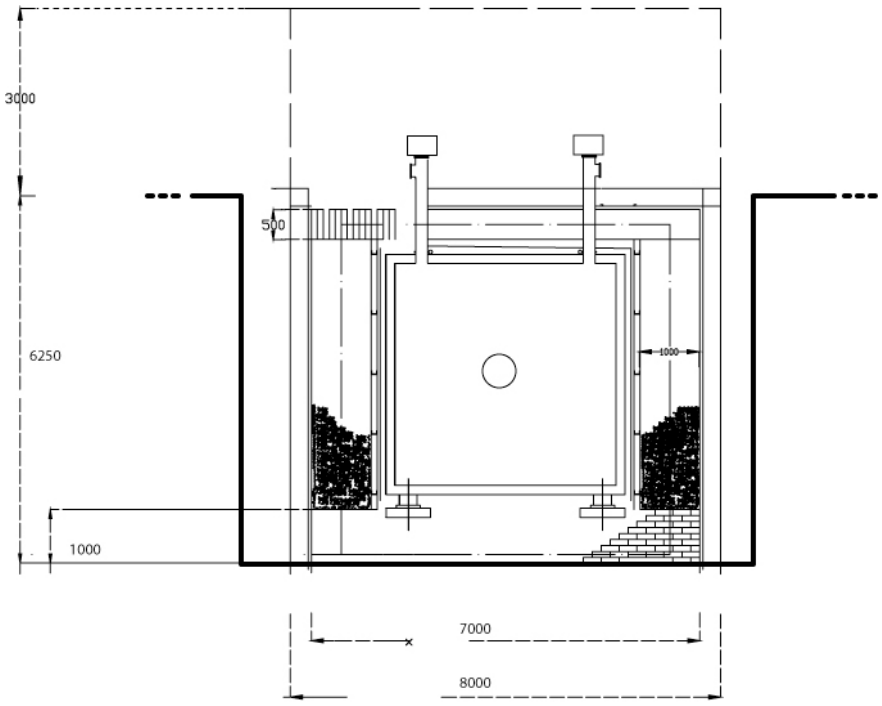

Figure 21. General layout of the new T150 LAr detector "cloned" from the ICARUS detector in the Close Position in Hall B-181 at CERN.

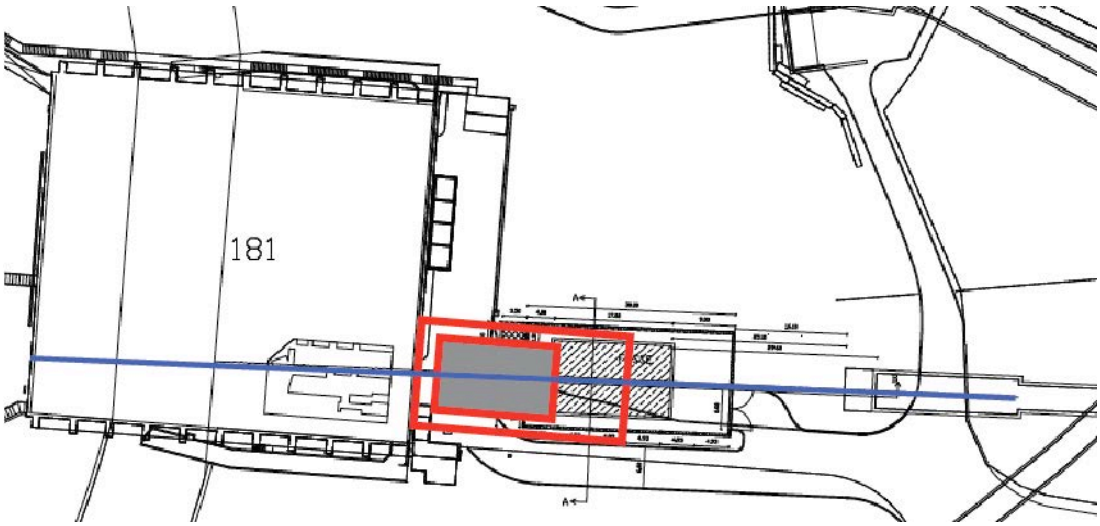

Figure 22. Possible layout of the pit for the T150 LAr detector. The original location in Hall B-181 is shown as well as the new possibility in an independent hall [20]. A possible intermediate location is also shown in red.

The neutrino beam crosses the pit at a height of about 3 m above the floor. Electronics will be installed on top of the detector at floor level. The

cryogenic equipment will be located close to the detector pit, on a surface of about 10 x 10 m^2. In particular, the wires, of a maximum length of about 10 m, will be anchored by special holders onto the wire frame in groups of 32 units (the wire modules). Only one set of horizontal wires (1056 units), about 10 m long, forms the induction-1 plane, stretched between the vertical beams of the wire frame; in both the induction-2 and collection planes (wires inclined at ± 60°) the standard length of the wires stretched between the upper and lower beams of the frame will be 3.77 m (~ 1900 wires per plane), while wires of decreasing length (960 wires per plane) will be used in the triangular-shaped portions, between one vertical and one horizontal beam, at the corners of the planes. Total number of wires is about 14200.

All the other components of the detector, cryogenic elements, internal photomultipliers, front-end electronics and read-out system, DAQ and ancillary equipment, will have to be replicated keeping in mind the down-scaled detector mass. The overall required electric power is less that 250 kW.

2.8 Cryogenic plants

Each T300 module is equipped with two gas-Argon and one liquid-Argon recirculation systems, required to attain a very high free-electron lifetime (several ms) in less than one month.

The continuously active gas recirculation units (≈ 25 GAr Nm^3/h each at maximum rate) collect the gas from the chimneys that host the cables for the wire chamber read-out. The gas is re-liquified into a LN_2 re-condenser with the liquid dropping into an Oxysorb/Hydrosorb filter placed below the re-condenser. The purified Argon is sent back into the LAr container just below the LAr surface. Similarly the liquid recirculation units (~ 2 LAr m^3/h) consist of an immersed, cryogenic, liquid transfer pump placed inside an independent dewar. The circulated LAr goes through standard Oxysorb/Hydrosorb filter before being re-injected into the cryostats. All ancillary cryogenic equipment will be dismounted at LNGS, transported individually and reinstalled at CERN.

The T150 module will be equipped with a similar cryogenic plant. In particular the LN2 re-condensation system will be equipped with a pair of the 12 Stirling cryo-coolers already operating at LNGS.

2.9 PMT system upgrade

The PMT electronic system makes use of analogue signal adders. For each chamber, all the PMT signals are summed and then integrated over several μ's, to take advantage of both, fast and slow, components of the scintillation light. Assuming the present PMTs layout and characteristics in the T600 detector at CERN, the efficiency for light collection in the PS beam has been evaluated using data with cosmic muons at LNGS. Full trigger efficiency for

ν_μ and ν_e charged current events is expected over the whole PSNF energy spectrum. For neutral current events the efficiency is rapidly growing above 90 % for $E_\nu > 0.7$ GeV in the fully PMT-equipped cryostat, while a 10 % lower efficiency is available in the partially equipped cryostat (Figure 23).

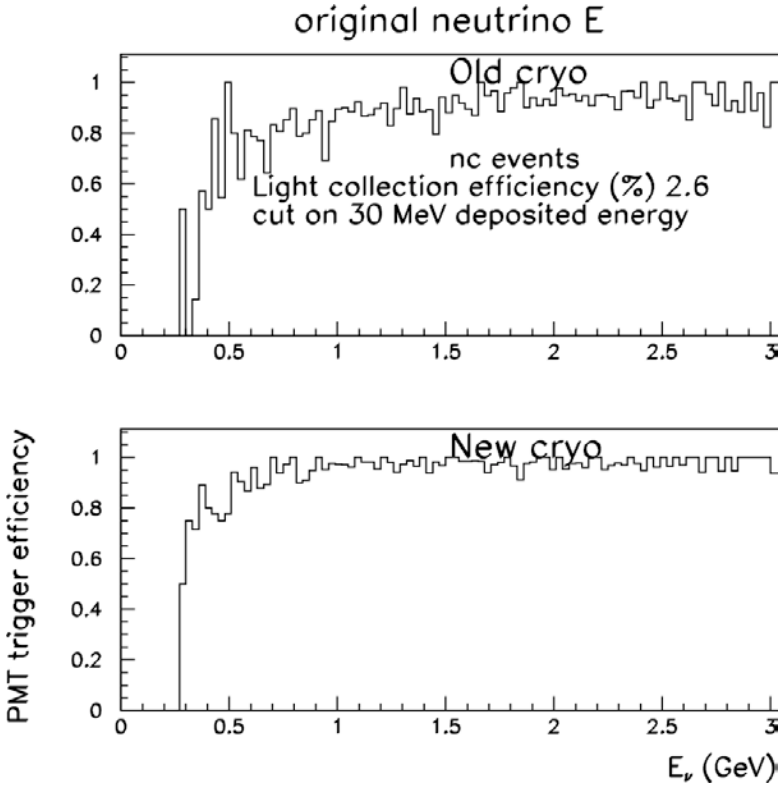

Figure 23. Trigger efficiency vs. deposited energy for PSNF ν neutral current events and with the present T600 detector. For PSNF ν_μ charged current events, the efficiency is 100% over the whole energy spectrum.

Although these results show that these efficiencies are high enough to collect almost all the events, some improvements of the light detection system can be foreseen for the T600 detector, to approach full efficiency in both cryostats down to tens of MeV. In addition each PMT time response can be sampled and stored using pattern recorders. The time sequence of ionizing events extracted from the PMT pattern will be useful for Region of Interest (ROI) identification and for residual cosmic background rejection during data analysis.

Additional improvements in the T600 detector can be achieved by replacing all the PMTs with new devices, such as the 8 inches Hamamatsu R5912MOD™, characterized by a better performance at cryogenic temperatures (Q.E. ~ 20%) with respect to the ETL models.

In the new T150 detector a PMT layout similar to that of T600 will be adopted, deploying about 30 Hamamatsu R5912MOD™ PMTs behind each wire chamber.

2.10 Electronics, DAQ, trigger system and data handling

The ICARUS T600 Front End electronics is based on an analogue front-end followed by a multiplexed 10-bit AD converter and by a digital VME module that performs local storage and data compression ([27, 28]). It is installed on the top of the cryostats, connected to the TPC wires through custom made feed-through mounted in UHV grade flanges. The overall architecture based on VME standard and performance are perfectly adequate for the proposed experiment, nevertheless possible improvements could always be implemented, being the whole electronic chain fully accessible.

The new T150 detector requires the implementation of ~ 14200 new electronics channels, based on the same analogue front-end amplifier used in the T600. The only change will be the adoption of a smaller package for the BiCMOS custom amplifier, dual channel, part of the front end, which is already available.

The same architecture of T600 will be adopted also for the digital part, with some relevant changes concerning the implementation, because most of the present components are no more available in the market.

Performance of the read-out system can be improved replacing the VME (8 - 10 MB/s) and the sequential order single board access mode inherent to the shared bus architecture, with a modern switched I/O, as PCI Express standard for instance, allowing the parallelization of the data flows. In addition such I/O transaction can be carried over low cost optical Gigabit/s serial links.

For T600 detector a very reliable and cost effective flange has been developed. Presently it allows for the connections of 18 cables, twisted pairs, and each conveying 32 signals from wire chamber to external electronics. It is conceivable to transform the external side of the flange in a sort of backplane, that support both analogue and digital electronics, with a compact design to house the full electronics on the flanges. The overall cost will be drastically reduced.

The event building architecture of the T600 is based on a network characterized by a two level switching layers, as shown in Figure 24. CPU's on the readout crates are connected through a 100 Mbps Fast/Ethernet link to a first 24 ports switch. A central 1 Gbps Giga/Ethernet switch then connects all the local switches to the PC farm.

The layout provides a receiving and merging workstation handling each readout chamber (24 readout units), with a maximum input throughput of ~ 50 MB/s and safely exploiting the link at half of the available bandwidth. All the readout units can work autonomously, pushing their own data to the receiving workstation. Segmentation and parallelization of the data

stream (e.g. 12 readout units per builder unit) allow reaching a building rate > 1 Hz on the whole T600, largely adequate to match the PS extraction rate.

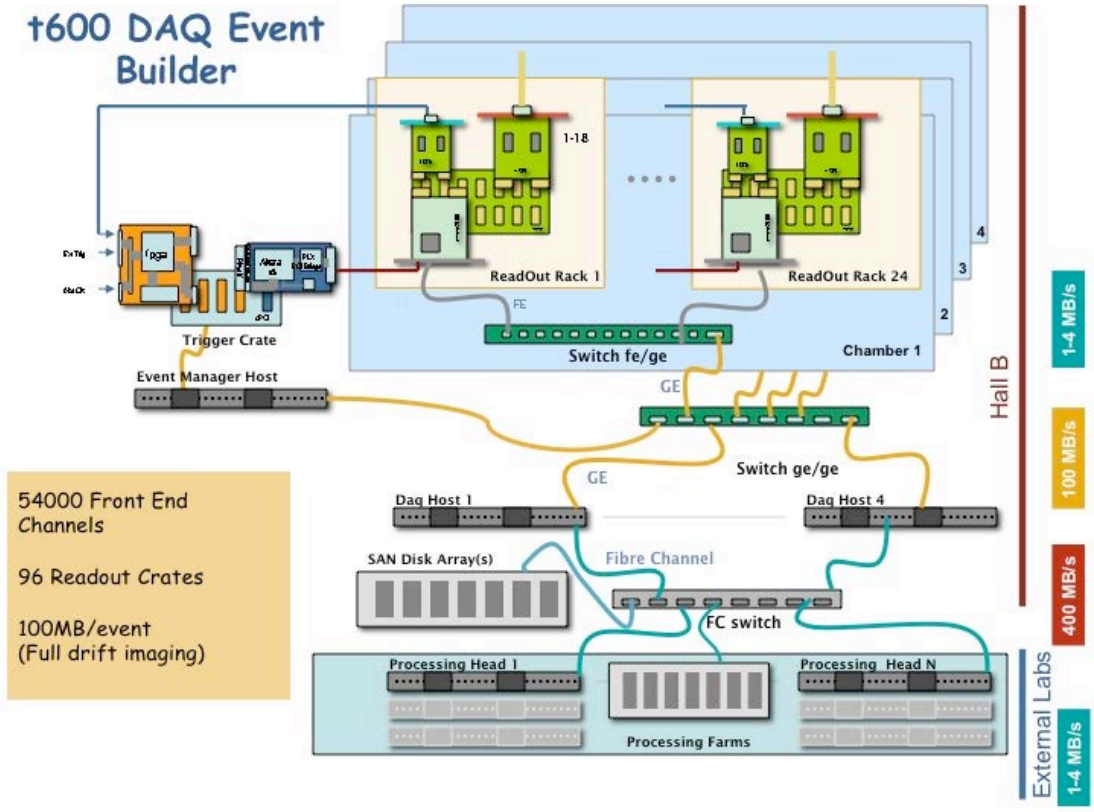

Figure 24. The T600 Data Acquisition system architecture.

The same DAQ architecture will be implemented in the T150 detector at the Near site. The trigger system will exploit the spill gate in coincidence with the signals of the PMT of each TPC.

At the nominal beam power, ~ 0.15 neutrino interactions per spill with vertex in the LAr-TPC's are expected in the Far position, with a slightly lower rate of beam related through going muons. Therefore the coincidence of the PMT signals within the spill will be used to trigger events acquisition in the T600.

Because of the expected high rate of neutrino interactions in the T150 detector (more then 1 event/spill), the beam gate alone will be used to trigger the data collection.

According to the maximum PS repetition rate (1 spill/1.2 s), ~ 70000 trigger/day on the near detector and ~ 15000 trigger/day on the far detector are expected. The corresponding data volume is around 0.5 TB/day, recording only the TPC where the event is localized and assuming the present data compression algorithms. This is comparable with the present T600 data-taking throughput. Moreover in both the Near and Far detectors, the DAQ system will benefit of the Region of Interest (ROI) search performed on-line

with the Super-Daedalus chip which allows to reduce considerably the quantity of data per event to be read-out and saved.

Data handling basic operations (e.g. data quality monitoring, prompt reconstruction, event tagging) and data streaming to a central facility (for instance: CASTOR @ CERN) will duplicate the present T600 scheme based on local live buffering disk space.

3 Signal selection and background rejection

A key issue of the proposed experiment is the LAr-TPC detection capability, where all reaction channels with electron production can be analysed without the need to restrict the search to the quasi-elastic channel, which accounts for about one half of the events (Figure 25). Moreover, events due to neutral currents are also very well identified and can be rejected to a negligible level. The energy resolution and detector granularity are largely adequate for the low energy range (0.1 ÷ 3 GeV) relevant for the present proposal. Extensive technical runs have been already performed by the ICARUS Collaboration both at surface level with cosmic rays in Pavia and exposed to the CERN WANF neutrino beam, and in the Gran Sasso INFN underground Laboratory (LNGS) exposed to the CNGS neutrino beam.

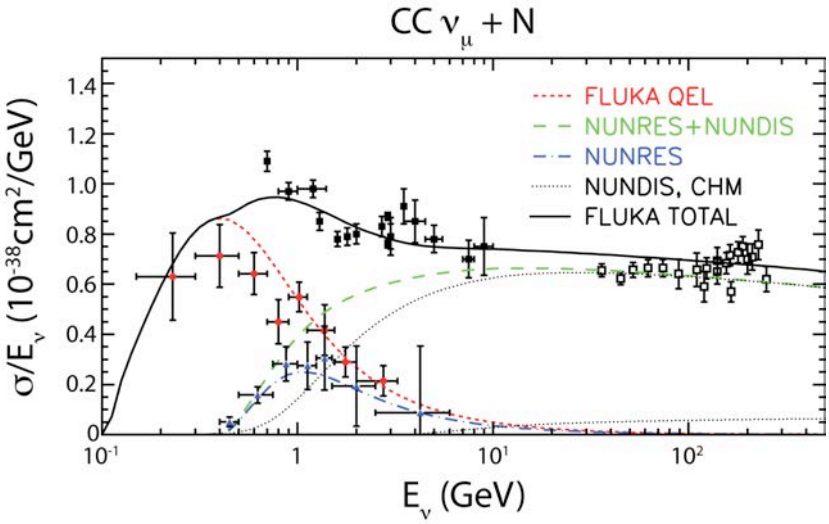

Figure 25. Total cross section for CC ν_μ-N interactions as a function of the incident neutrino energy. The various contributions from the FLUKA calculations are explained in the figure. Charm production is displayed separately, but is part of the NUNDIS event generator. Refer to [34] for details on experimental data.

3.1 LAr-TPC observed performance

The performance of the LAr-TPC has been already demonstrated with data from past prototypes and from the 2001 T300 technical run performed with cosmic rays on surface [27]. The electromagnetic energy resolution in the sub-GeV energy range is $\sigma(E)/E = 0.03/\sqrt{E(GeV)} + 0.01$, in agreement with π^0 invariant mass measurements [30]. At higher energies the estimated resolution for hadronic showers is $\sigma(E)/E = 0.30/\sqrt{E(GeV)}$. However the LAr-TPC detector allows identifying and measuring, track by track, each hadron produced in low energy neutrino interactions, through ionization and range, leading to a much better energy resolution. A number of physical features of the LAr-TPC, relevant for the present proposal, as obtained from the experimental data, are shown in Figure 26 (A to F).

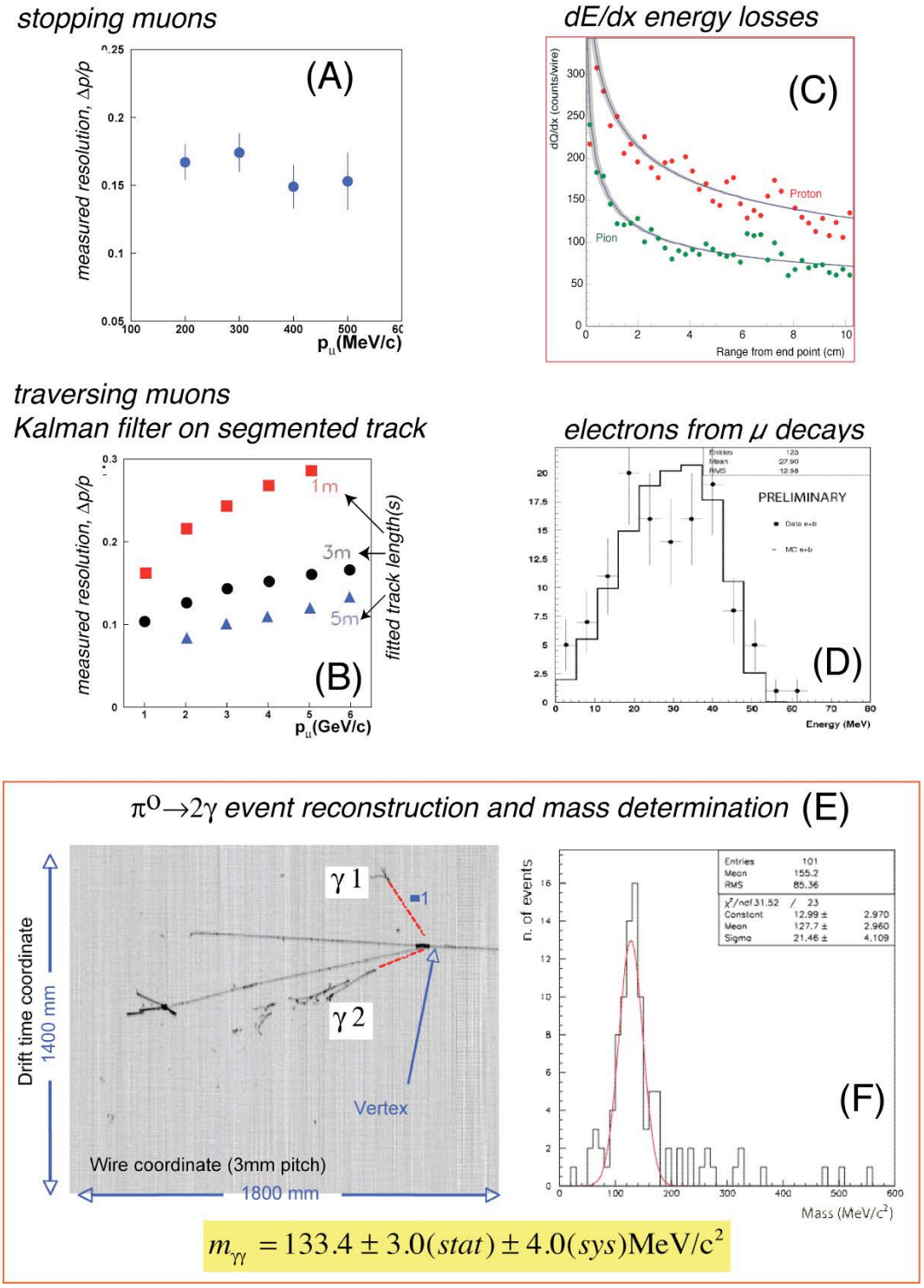

Figure 26. Experimental results from the T300 Pavia ICARUS run (A) momentum resolution of stopping muons; (B) momentum resolution of traversing muons with the Kalman filter method; (C) dE/dx energy loss for slow pions (green) and protons (red); (D) Michel electron decay spectrum from $\mu \rightarrow$ e decays; (E) $\pi^o \rightarrow 2\gamma$ event reconstruction and mass determination; and (F) mass spectrum of 230 interactions with $\gamma\gamma$ candidates.

The momentum of muons can be determined through the reconstruction of multiple Coulomb scattering inside the detector. This method has been verified by comparison with the integrated energy loss of stopping mu-

ons from the cosmic rays test. The Kalman filter method has been used, applied to segmented tracks (L_{seg}: segment length). The resulting momentum was then extracted from the deflection angle θ and from χ^2 of the fit. A resolution $\Delta p/p = 15\%$ due to multiple scattering [31] has been obtained for energies up to 0.5 GeV (Figure 26A). The procedure, thus validated, has been extended to higher energy with MC calculations; the resolution $\Delta p/p$ can be as good as 10%, depending mainly on track length (Figure 26B).

The measured *dE/dx* energy losses for pions and protons are shown in Figure 26C. Clear separation of the nature of the particle is easily obtained from the last part of the residual range.

In Figure 26D is reported the excellent resolution obtained from the decay electron spectrum (Michel parameter) from muon decays, collected with the T300 technical run exposure [32]. The bremsstrahlung losses have been included.

The reconstruction of a typical $\pi^0 \rightarrow 2\gamma$ event from the T300 technical run is shown in Figure 26E; both γ's converting away from the hadronic vertex have been identified, associated and measured. Finally in Figure 26F 230 hadronic interactions with γγ candidates selected from T300 Pavia run are shown. A prominent π^0 peak is found with an invariant mass of 133.4 ± 3.0 ± 4.0 MeV/c^2 [30]. The average γ conversion length is (17.4 ± 0.8) cm, in agreement with the expectation of 18 cm.

Quasi-elastic neutrino events in LAr have been reconstructed in the 50 litre ICARUS LAr-TPC exposed to the CERN-WANF beam in coincidence with the NOMAD experiment [33]. In Figure 27 two events are shown: (A) a quasi-elastic proton recoil event, a typical topology of the present Proposal as well; (B) a multi-prong event. Both events can be readily reconstructed in 3D with particle identification, momentum balance and π^0 rejection. We notice that in this exposure only two views were available, and the reconstruction will be easier with the three views of the present T600.

Finally in Figure 28 a selection of ~ 200 pure lepton-proton final state events from the 50 litre ICARUS LAr-TPC with exactly one proton with kinetic energy $T_p > 50$ MeV (range > 2 cm) and any number of protons with $T_p < 50$ MeV is presented. There is a good agreement with FLUKA expectations, accounting for Nuclear Fermi motion and re-interactions in nuclei [24].

3.2 ICARUS-T600 run at LNGS

The software tools for reconstruction and analysis are presently developed and tested on the events recorded by the T600 detector at LNGS underground laboratory exposed to CNGS neutrino beam. The 2010 data sample is being used as a training sample to tune the reconstruction, check calibration and optimize the identification and measurement algorithms.

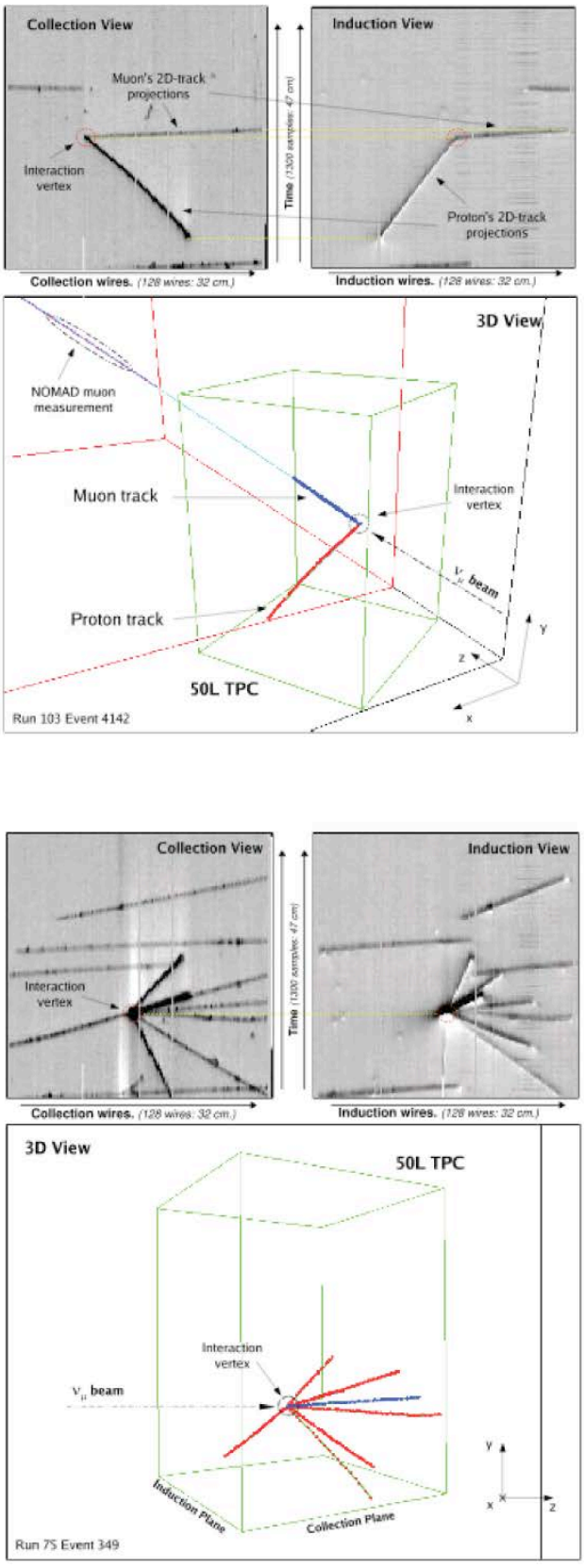

Figure 27. Events from a 50 litre ICARUS TPC exposed to the CERN-SPS neutrino beam in coincidence with the NOMAD experiment: (A) a quasi–elastic event with a muon and a proton recoil track; (B) a complex multi-hadron event. In both events a 3D reconstruction is shown.

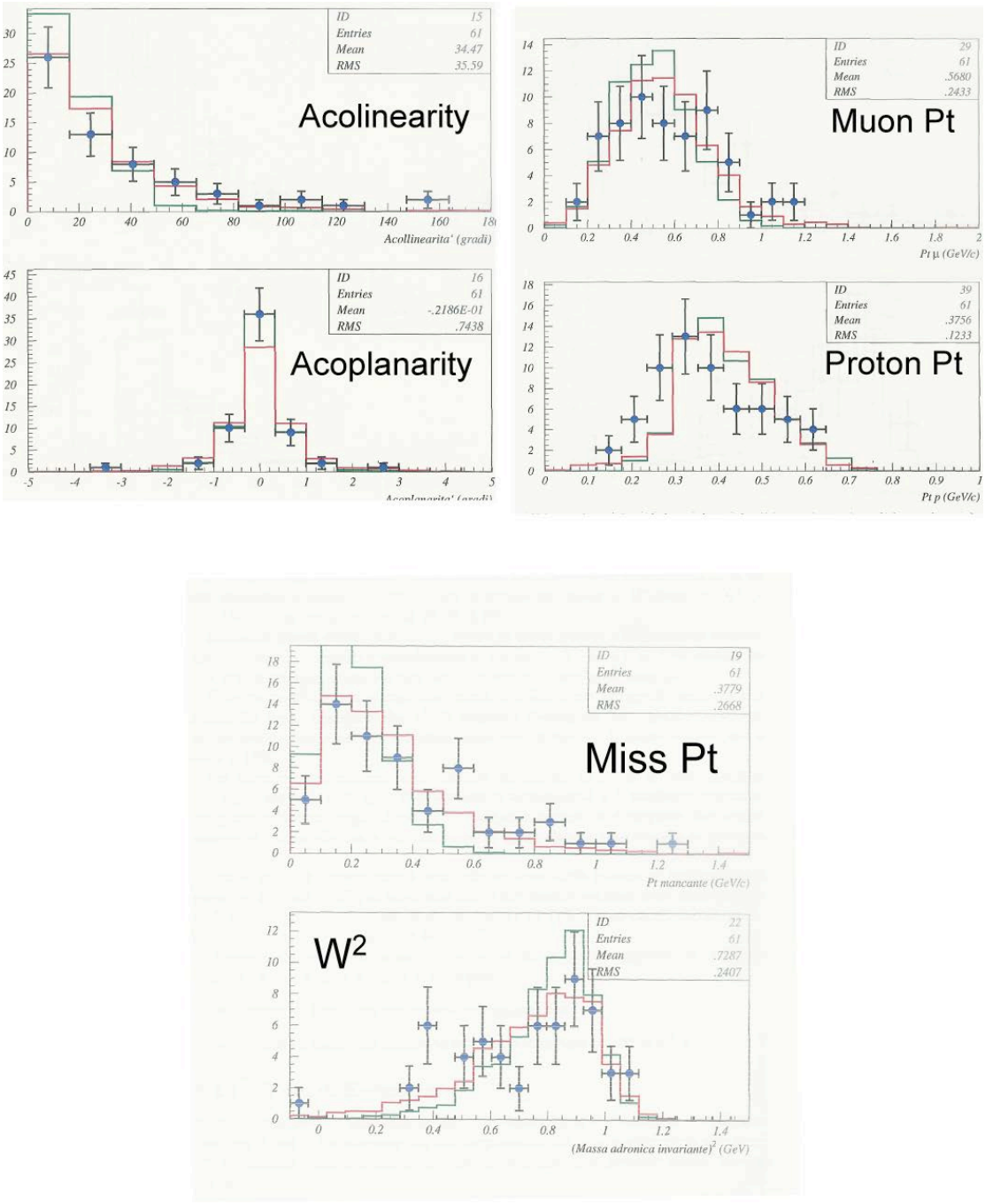

Figure 28. Selection of ~ 200 pure lepton-proton quasi elastic final state with exactly one proton with kinetic energy T_P>50 MeV (range > 2 cm) and any number of protons with T_P <50 MeV. Good agreement with FLUKA expectations (Red line), accounting for Nuclear Fermi motion and re-interactions in nuclei.

The 3D track reconstruction starts from a 2D track finding algorithm based on an automatic clustering over an angle-position matrix. A segment-based approach has been developed for three-dimensional reconstruction. The information from track reconstruction feeds the algorithms for muon momentum determination through multiple scattering, and for particle identification.

The application of the multiple scattering method to the 2010 data is shown in Figure 29, where the reconstructed momentum distribution is compared with the Monte Carlo predictions for CNGS ν_μ CC events. The average reconstructed momentum is 11.5 ± 1.8 GeV/c in agreement with the expected value of 12.4 GeV/c.

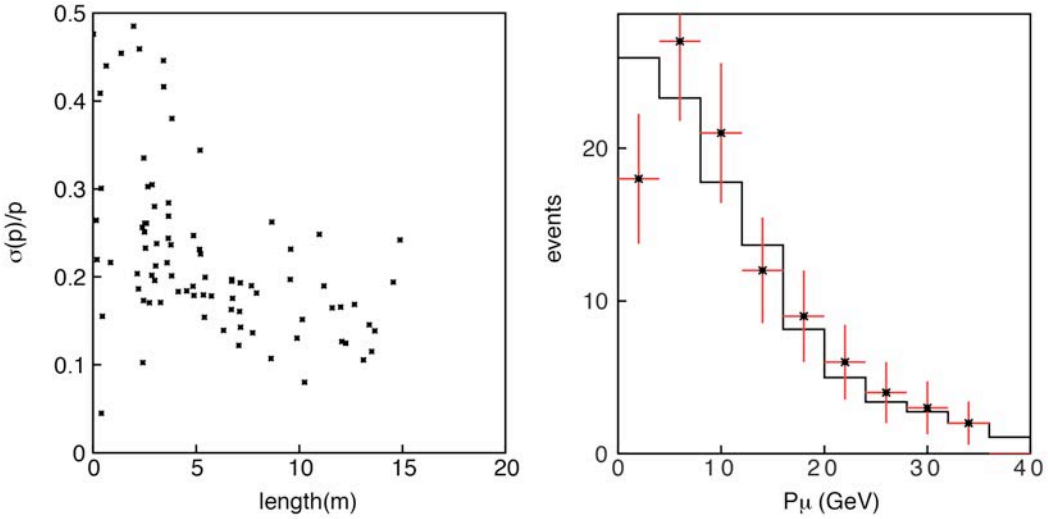

Figure 29. Application of the multiple scattering reconstruction to CNGS events. Left: momentum resolution as a function of track length. Right: reconstructed momentum (dots with red error bars) compared with the Monte Carlo expectations (black line).

Charged particle tracks are reconstructed in three dimensions with the help of polygonal line algorithm. Particle identification is performed both with topological considerations (for example decay products) and with the reconstruction of dE/dx versus range. For this last purpose, a method based on neural network is used. Corrections to recover the ionization quenching are applied to the reconstructed energy loss. An example of stopping particle identification is shown in Figure 30.

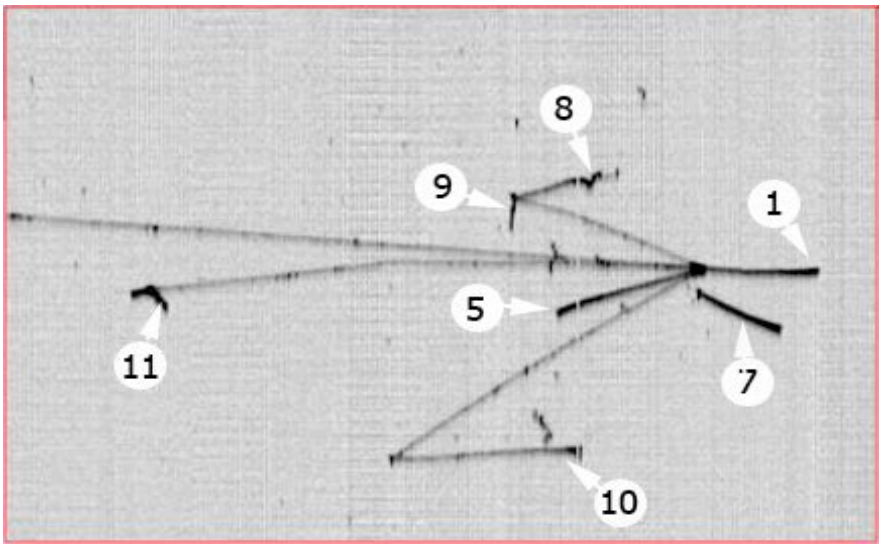

Figure 30. Example of stopping particle identification in a CNGS ν_μ CC event. Track n.8 is a pion, the other numbered tracks are protons.

The present reconstruction procedure applied to one CNGS muon neutrino event is shown in Figure 31. The expected capabilities of the detector to distinguish between electron showers and neutral pion decays are also tested: all the ingredients are indeed present in the observed events. Despite the statistics too low to produce distributions, all the reconstructed invariant masses agree with that of the pion within errors, except for an example of η decay (reconstructed mass is 512 ± 48 MeV). Conversion distances range from few centimetres to about 80 cm, and the initial ionization is always consistent with two m.i.p.s. An example with two π^0 is also shown in Figure 32.

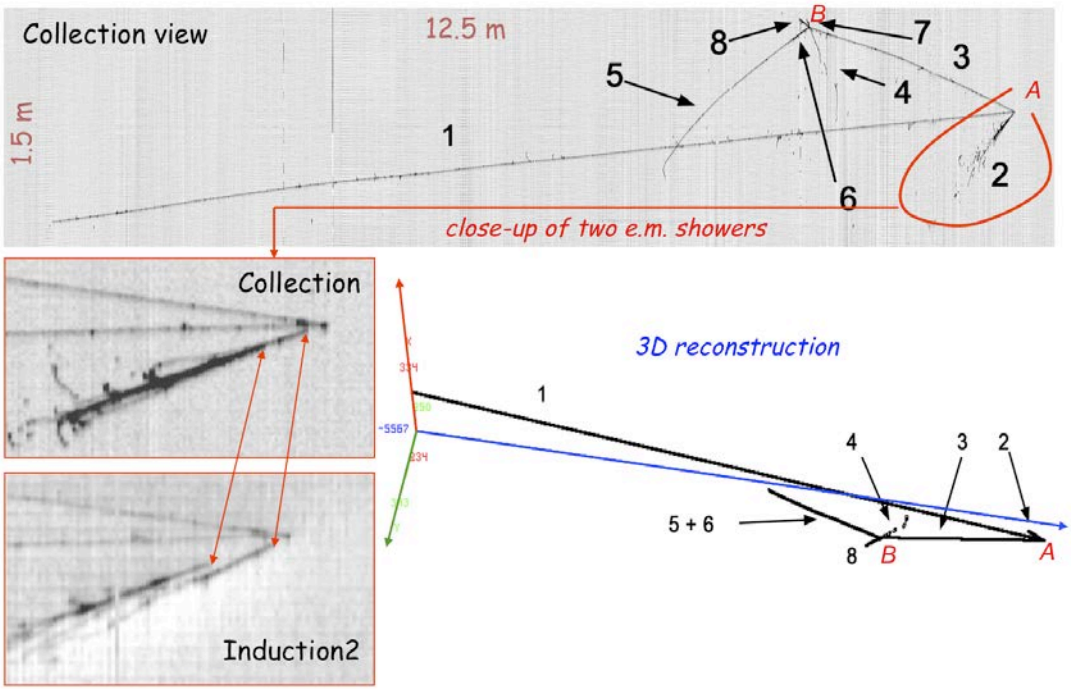

Figure 31. CNGS beam related muon neutrino event fully reconstructed. Primary vertex (A): very long leading μ (1), e.m. cascade reconstructed as a neutral pion (2), charged pion (3). Secondary vertex (B): the longest track (5) is a μ coming from stopping k (6). The μ decay is also identified. All particle momenta are measured for a complete kinematic reconstruction of the event.

The full 3D reconstruction of all particles in the events allows determining the neutrino momentum and the missing transverse momentum in the interaction. In addition, a calorimetric reconstruction is also possible. The calorimetric reconstruction of the energy deposited in the detector by ν_μ CC events shows a nice agreement with expectations (Figure 33).

The deposited energy in each event is corrected for quenching on average, and a further correction for non-containment and non-compensation is applied. This correction has been computed from Monte Carlo simulations and depends on the vertex position in the detector. For CC events, the energy deposited by the muon is subtracted from the total, and muon momentum is anyhow reconstructed by multiple scattering. As a first check, the raw ener-

gy distribution, after the quenching correction only, has been successfully compared with the expected one.

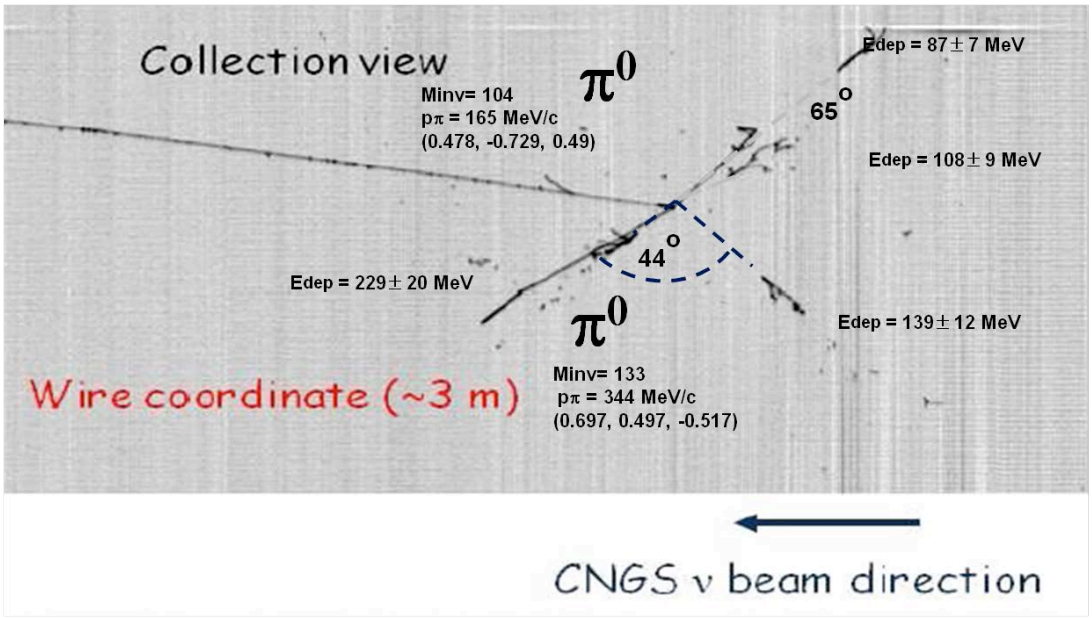

Figure 32. Example of π^0 identification in a CNGS ν_μ CC event. The conversion distances are: 71.2 cm, 13.7 cm, 41.8 cm, 17.4 cm and the initial ionization are 5.1, 6.1, 3.1 and 4.4 MeV/cm.

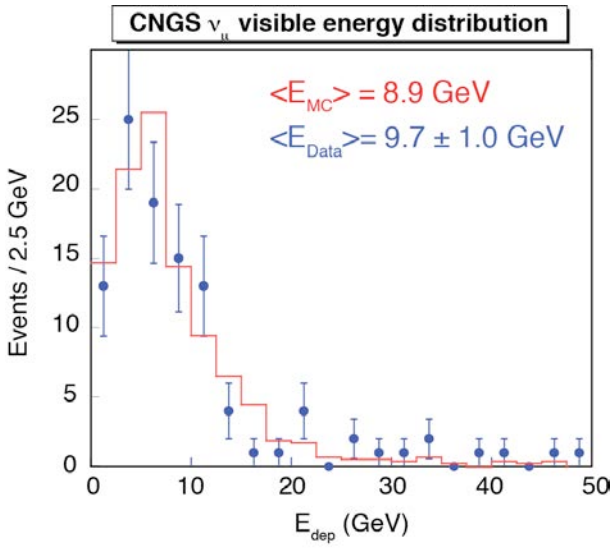

Figure 33. The energy deposited inside the detector in ν_μ CC events (calorimetric method, quenching corrected).

The reconstructed neutrino spectrum, obtained from the combination of muon momentum and calorimetric energy, is shown in preliminary version in Figure 34. The agreement with the predicted ν_μ spectrum is satisfactory.

Cosmic events have been identified by means of an automatic identification and reconstruction procedure. The region of the detector containing the events is identified in Collection view and the deposited energy determined taking into account the present electron lifetime and quenching cor-

rections. The results compare well with the Monte Carlo predictions for the spectrum of the energy deposition by cosmic muons, as shown in Figure 35. Simulations include an energy dependent correction to account for the present trigger efficiency.

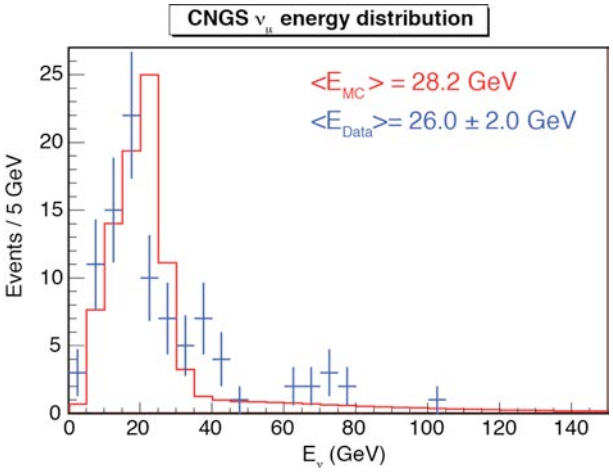

Figure 34. Reconstructed neutrino energy spectrum from ν_μ CC events, with the calorimetric method, compared with expectations.

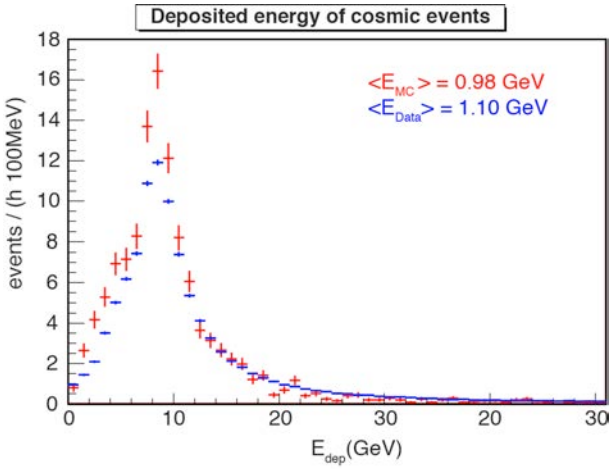

Figure 35. Calorimetric measurement of the energy deposition by cosmic rays in the detector as determined by an automatic reconstruction (data points in blue, MC prediction in red).

As shown in the previous examples the analysis tools to measure and fully reconstruct the events are working satisfactorily both for the detailed identification and measurement of all secondary particles from the ν interactions, for the reconstruction in the transverse plane and for a calorimetric like reconstruction.

Particle identification works well exploiting the dE/dx vs range dependency to separate different particles. Neutral pions are reconstructed as expected in individual events: the γ can be easily recognized and reconstructed matching in pairs the π^0 mass. All these features will be checked on the full data sample, as required to qualify the performance of the detector for the neutrino oscillation search. The first steps towards an automatic re-

construction of the events are in place, other tools are being developed in this direction.

3.3 Signal and background at the CERN PS experiment

A full simulation of the expected neutrino events in the LAr detectors for the proposed experiment has been performed within the FLUKA framework [34]. It must be stressed that especially at low energies the corrections due to the nuclear effects and Pauli exclusion principle are substantial [35]. However, these effects are the same and therefore cancel out when the spectra in the "Near" and "Far" positions are compared.

The number of events for the "Far" and "Near" detectors are given in Table 3 for $2.5\,10^{20}$ pot for $E_n < 10$ GeV. A beam intensity of $3x10^{13}$ protons/spill has been assumed. The event rates have been calculated according to the target and horn configuration described in section 2.1. Further optimization of the secondary beam optics is being performed, aiming to improve the neutrino yields.

In Figure 36 we show a ν_e CC interaction for a 1.5 GeV neutrino. The Monte Carlo simulation shows that the energy reconstruction of electron neutrino interaction events is not affecting the signal/background ratio if a minimal cut of 50 cm in the longitudinal direction and a 10 cm cut on the sides of the sensitive volume of each T300 is performed, corresponding to a fiducial volume of 90 % of the active one. Electron identification is also ensured under these geometrical cuts. Indeed, due to the directionality of the neutrino beam, the probability that an electron escapes from the instrumented volume before initiating a shower is extremely small: only 2 % of the electrons travel through a LAr-TPC thickness smaller than 3 X_0 and 0.3 % travel less than 1 X_0 in the instrumented volume. Within the previously described fiducial volume, the expected average neutrino energy resolution is about 14%.

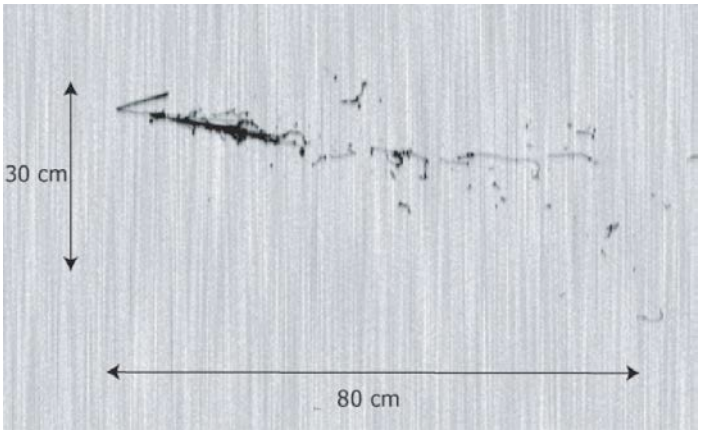

Figure 36. Collection view of a 1.5 GeV QE electron neutrino event. Note the presence of a singly ionizing electron immediately after the event.

Due to the excellent imaging capability of the LAr-TPC, π^0 from NC events are easily distinguished from electrons. First of all, events where both photon conversion points can be distinguished from the interaction vertex can be rejected. In the present analysis we assume that photons are immediately identified if the conversion distance is equal or larger than 2 cm. The remaining π^0 background is further reduced by discarding events where the parent π^0 mass can be reconstructed within 10 % accuracy. Only 3 % of π^0 survives the cuts for events with vertex inside the fiducial volume. The remaining photons can be discriminated from electrons on the basis of dE/dX analysis. Since photons convert mainly through pair production, the ionization at the beginning of the shower corresponds to that of two electrons. A few wires are enough to distinguish the signal from a single m.i.p. or two m.i.p.s. This method provides 90 % electron identification efficiency with photon misidentification probability of 3 % (Figure 37). The latter is mostly due to photons undergoing Compton scattering, whose branching fraction at these energies is of the order of the percent. The final π^0 mis-interpretation probability is 0.1 %, the corresponding electron neutrino detection efficiency is 90 % within the fiducial volume.

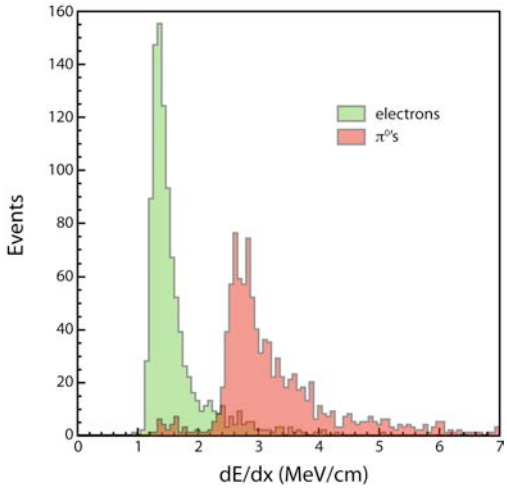

Figure 37. Expected electron - π^0 separation in the LAr-TPC using ionization measurements along tracks in the vertex region.

The simplest, uncorrected, calorimetric reconstruction of the deposited energy is shown in Figure 38 for two sets of oscillation parameters. The difference in shape is already visible at this stage of the reconstruction, as well as the huge reduction of the background due to neutral current events.

As an important feature of the present proposal, the run with anti-neutrino beam has been included in order to further check the LSND claim, which is mainly based on anti-neutrino data. Switching the horn polarity to select negatively charged mesons results in an anti-neutrino beam with total fluence of 68 % with respect to the neutrino mode. The energy spectrum is similar. The wrong-sign (ν_μ) component is enhanced due to forward going positive mesons that escape the horn defocusing. The resulting event rate is

17 % of that collected in neutrino mode. This reduction is due to the larger impact of nuclear effect on the anti-neutrino interactions, where the momentum transfer is smaller.

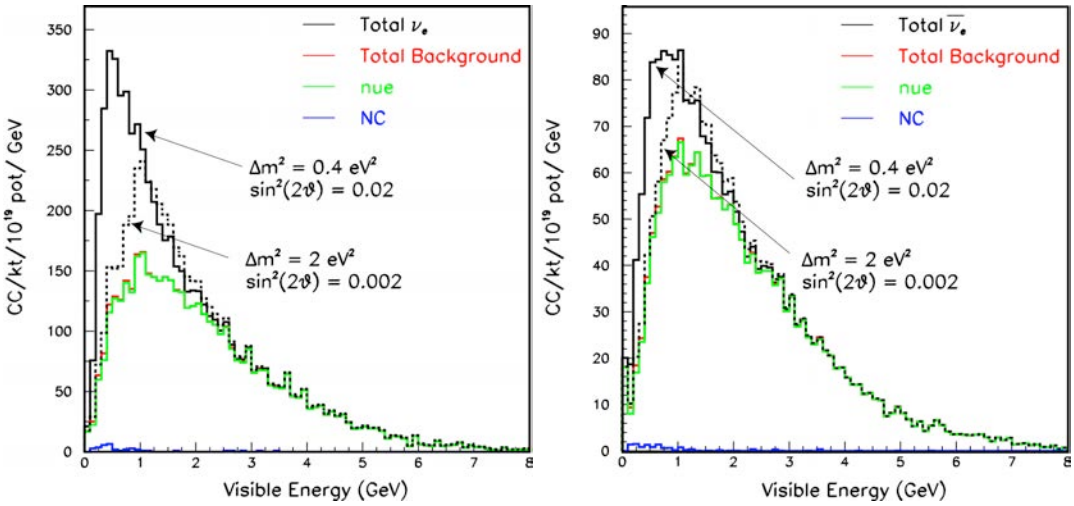

Figure 38. Deposited energy spectra for electron-like events in the Far detector for neutrinos (left) and anti-neutrinos (right).

Because of the same reason, the ν_μ component is strongly enhanced. Event rates in the CERN-PS beam for the un-oscillated spectra and a few $\nu_\mu \rightarrow \nu_e$ oscillation values are reported in Table 3. Examples of the expected energy deposition spectra are shown in Figure 38-right.

Possible background to ν_e and anti-ν_e due to cosmic ray photons entering the detector without accompanying charged particles has been investigated. A rough estimation of the rates foresees that ≈ 0.1 such photon with energy greater than 500 MeV impinges on the detector within the 1 ms drift time. Such a background can be easily removed since:

i) As for π^0 rejection, the showers initiated by photons can be identified through the specific ionization in the first centimetres. Few residual singly ionizing events are due to Compton scattering, which in this energy range occurs with a probability of about 10^{-2} with respect to pair production.

ii) It peaks in the downward vertical direction while genuine events point to the beam direction. It is possible to reject to about 10^{-3} cosmic photon with negligible reduction of efficiency for ν_e CC.

iii) The γ interaction length in LAr is λ_R = 14 cm, and the length of not instrumented LAr crossed by γ close to beam direction exceeds 1 m, reducing the background by a factor ≈ 0.5 x 10^{-3}.

iv) The ν_e event is producing also at least one hadron (proton, neutron, nuclear star if quasi elastic, plus a π if inelastic), while the Compton γ-

ray is recoil-less. The total amount of observed ionization in the immediate vicinity of the vertex can signal the presence of a ν-related event. The presence of a charged π or of a proton is an unambiguous signature, which cannot be missed. The presence of a neutron is more difficult since λ_I = 80 cm, although a sizeable local neutron star is expected in about 90% of the events.

In conclusion the rejection capability of the CR gamma events is about 5 x 10^{-9}. Since the occurrence of these events is about 1 every 10 beam pulses, the resulting background is negligible when compared to the expected ν_e CC (≈ 10^{-3} per spill) in the far detector. Additional rejection can also be obtained from timing information provided by the PMTs.

Table 3. Number of events for the "Far" and "Near" detectors given for 2.5 10^{20} pot for E_ν < 10 GeV. The oscillated signals are clustered below 3 GeV of visible energy. A beam intensity of 3x10^{13}protons/spill has been assumed.

	ν focus		$\bar{\nu}$ focus	
	FAR	NEAR	FAR	NEAR
Active mass	476 t	119 t	476 t	119 t
Distance from target	850 m	127 m	850 m	127 m
ν_μ CC interactions	9.7 x 10^5	8.5 x 10^6	6.6 x 10^4	5.2 x 10^5
$\bar{\nu}_\mu$ CC interactions	1.1 x 10^4	9.0 x 10^4	1.6 x 10^5	1.2 x 10^6
QE ν_μ + $\bar{\nu}_\mu$ interactions	4.5 x 10^5	4.1 x 10^6	1.0 x 10^5	8.6 x 10^5
CC Events/Burst	0.12	1.0	0.03	0.21
Intrinsic ν_e + $\bar{\nu}_e$ from beam	6900	6.2 x 10^4	2800	3.0 x 10^4
Intrinsic ν_e + $\bar{\nu}_e$ (E_ν < 3 GeV)	4400	4.3 x 10^4	1850	2.1 x 10^4
ν_e oscillations:				
$\Delta m^2 = 2.\ eV^2;\ sin^2 2\theta = 0.002$	1300	1800	290	300
$\Delta m^2 = 0.4\ eV^2;\ sin^2 2\theta = 0.02$	2800	850	530	150
$\Delta m^2 = 0.064\ eV^2;\ sin^2 2\theta = 0.96$	4450	1050	870	190
$\Delta m^2 = 4.42\ eV^2;\ sin^2 2\theta = 0.0066$	2860	19500	650	3400

The possibility to install the near detector in a new building located slightly upstream of the originally proposed location is being investigated. The rate of events in the near position largely exceeds the required number of events when compared with the ones of the Far position.

Therefore in case the rate would turn out to be excessive, the possibility exists of reducing periodically (once every few pulses) the beam intensity in order to make the topologies in the two detectors more similar to each other.

An important feature of the present proposal is the large statistics of neutrino interactions, which can be collected. This is possible by the LAr-TPC detection technique, which allows the reconstruction of the totality of

neutrino interactions without restricting to the QE interactions and to realize absolutely homogeneous detector of large mass. The adopted neutrino beam energy permits, unlike lower energy beams, to obtain useful neutrino rates, also operating in antineutrino mode.

4 Sensitivity to oscillations

As already described, our proposal at the CERN-PS is based on the search for spectral differences of electron like events in two identical detectors, 850 m and about 127 m away from the source.

The beam produced by the PS protons can be set separately to produce neutrinos or antineutrinos. Important unaccounted differences, being hinted between these two neutrino species, which may even be related to a failure of CPT symmetry, can be addressed with this experiment.

The ν_e and $\bar{\nu}_e$ beam components are produced by the three body decays of K and μ. As shown in Figure 10, the spectral distributions are extremely similar at the far and near positions. The intensity of the ν_e signal is much smaller than the one of the dominant ν_μ's, however it is largely sufficient to collect an adequate number of events. The signature of charged currents ν_e events is extremely clean because of the unique "bubble chamber like" quality of the events produced by the LAr-TPC and the sensitivity of the experiment is enhanced by the close similarity of the two detectors.

In absence of oscillations, the two energy spectra should be a precise copy of each other. An exact proportionality between the two ν_e spectra implies directly the absence of neutrino oscillations. Any experimentally observed difference between the spectra of ν_e events at the two locations must be inevitably attributed to a time evolution of the neutrino species.

4.1 ν_e and ν_μ disappearance signals

The persisting presence of disappearance anomalies in reactor neutrino experiments, in the Gallex and Sage calibration with sources and in other experiments is an open challenge. As well known, these data may be well fitted by the 3 + 1 neutrino hypothesis, while the no-oscillation hypothesis is disfavored at 99.93% C.L. The presently proposed experiment is however intended to detect experimentally the oscillation pattern in the $\sin^2 2\theta_{new} - \left|\Delta m^2_{new}\right|$ plane, beyond the so far unaccounted lack of ν_e events. Both the ν_e and ν_μ disappearance signals may be searched for.

In Figure 39 the energy distributions of the electron neutrino events is shown for the "Far" (a) and "Near" (b) positions together with a number of possible $\left|\Delta m^2_{new}\right|$ value in the region of $\left|\Delta m^2_{new}\right| > 1\text{eV}^2$ and $\sin^2 2\theta_{new} \approx 0.16$. If confirmed, the existence of a new neutrino species carrying such a large mass will have an important role in the explanation of the existence of the Dark Mass in the Universe.

In Figure 40 the 90% confidence levels for the actual oscillation mechanism in the $\sin^2 2\theta_{new} - \left|\Delta m^2_{new}\right|$ plane are shown for the presently proposed

experiment with an integrated intensity corresponding to (a) 2.5 x 10^{20} pot (protons on target), corresponding to two years of data tacking at the presently available beam intensity, (b) to 7.5 x 10^{20} pot, or 2 years of dedicated data tacking and (c) to 22.5 x 10^{20} pot curve. They are also compared with the "anomalies" from the combination of the published reactor neutrino experiments, Gallex and Sage calibration sources experiments.

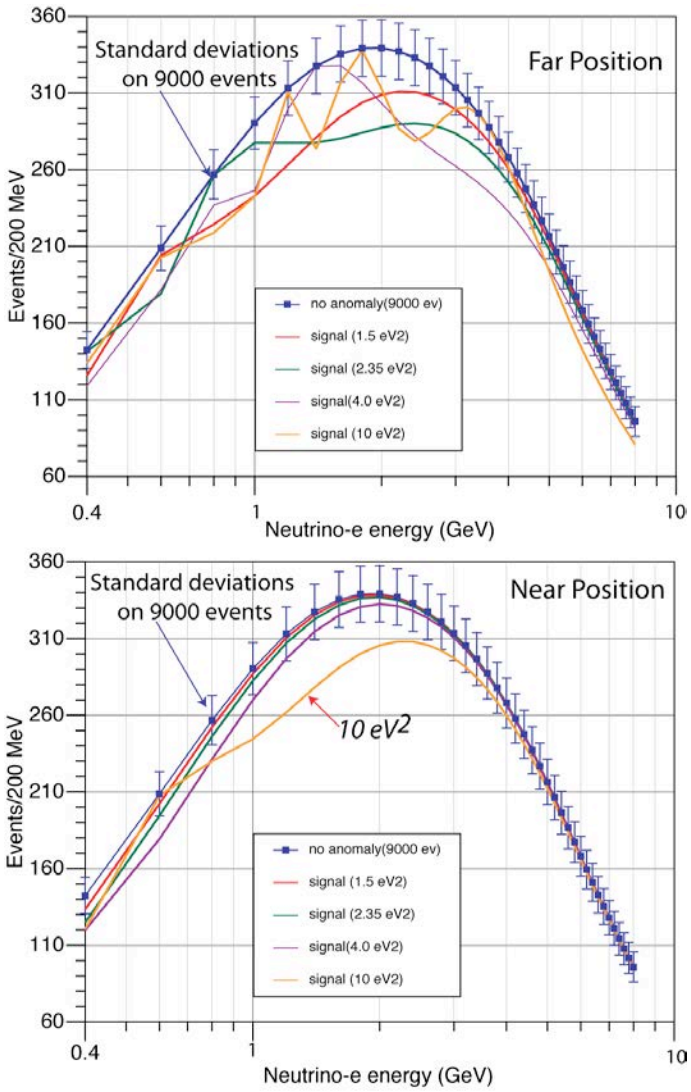

Figure 39. Energy distributions of the electron neutrino events in "Far" (a) and "Near" (b) detectors for a some $\left|\Delta m^2_{new}\right|$ values in the region E > 1eV^2 and $\sin^2(2\theta_{new}) \approx 0.16$.

The disappearance signal in the same $\sin^2 2\theta_{new} - \left|\Delta m^2_{new}\right|$ range may also be studied with the dominant ν_μ and $\bar{\nu}_\mu$ signals. The ν_μ and $\bar{\nu}_\mu$ spectral shapes, primarily due to pion decays, are significantly different in the "Near" and "Far" positions. In the energy range below 3 GeV, where the effect is expected, the relative differences amount to about 30% and they may be predicted to about 2%. This systematic uncertainty is larger than the statistical fluctuations expected for the huge number of collected events. However, the amount of ν_μ depletion should be large enough for a significant test.

Indeed, in sterile models the amplitude of the probability of appearance processes, like $\nu_\mu \rightarrow \nu_e$ transitions, are proportional to the product of two elements of the transition matrix. In disappearance processes, the amplitude is proportional to just one element of the transition matrix. For this reason much higher probabilities are expected in disappearance modes than appearance (something like first order with respect to second order effects). Amplitudes as big as 10 - 20% are expected in the ν_μ disappearance channel.

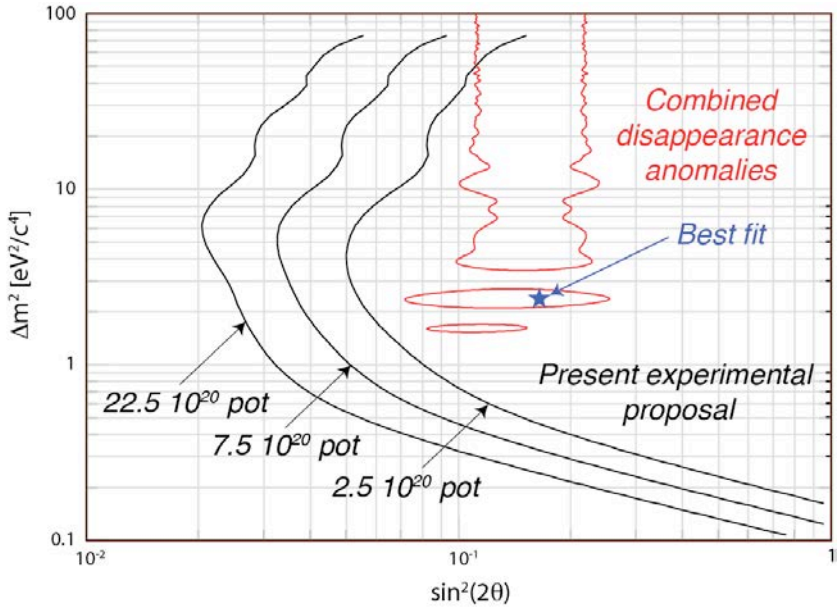

Figure 40. Oscillation sensitivity (90% C.L.) in the $\sin^2(2\theta_{new})$ - Δm^2_{new} plane for various integrated intensities of the refurbished PSNF. Combined disappearance "anomalies" from the published reactor neutrino, Gallex and Sage calibration sources experiments are also shown (red). A 1% overall and 3% bin-to-bin systematic uncertainty on the energy spectrum is included.

4.2 $\nu_\mu \rightarrow \nu_e$ appearance signal

A sensitivity of $\sin^2 2\theta_{new} < 3 \times 10^{-4}$ (for $|\Delta m^2_{new}| < 2\ \mathrm{eV}^2$) and $|\Delta m^2_{new}| < 0.02\ \mathrm{eV}^2$ (for $\sin^2 2\theta_{new} = 1$) at 90 % C.L. is expected with a two year exposure at the CERN-PS ν_μ beam (Figure 41-top). The parameter space region allowed by the LSND experiment is fully covered, except for the highest Δm^2 region. The sensitivity has been computed assuming a 3% systematic uncertainty in the "Far" to "Near" ratio prediction

In anti-neutrino focusing, twice as much exposure (5.0×10^{20} pot) allows to cover both the LSND region and the new MiniBooNE results (Figure 41-botton). Both favoured MiniBooNE parameter sets, corresponding to two different energy regions in the MiniBooNE antineutrino analysis, fall well within the reach of this proposal.

In Figure 42 a number of experimentally expected oscillation patterns at 850 m are shown for two neutrino (mu - e) oscillations and for some indicative positions of the LSND allowed region (indicated with a star mark). One can see that very different and clearly distinguishable patterns are indeed

possible depending on the actual values in the ($\sin^2 2\theta_{new} - |\Delta m^2_{new}|$) plane. It appears that the present proposal, unlike LSND and MiniBooNE, can indeed determine in the case of an observed effect, both the mass difference and the value of the mixing angle. In Figure 42 the intrinsic ν_e background due to the beam contamination is also shown. The magnitude of the expected oscillatory behaviour, although for the moment completely unknown, is in all circumstances well above the background, also considering the very high statistical impact of the experimental measurement.

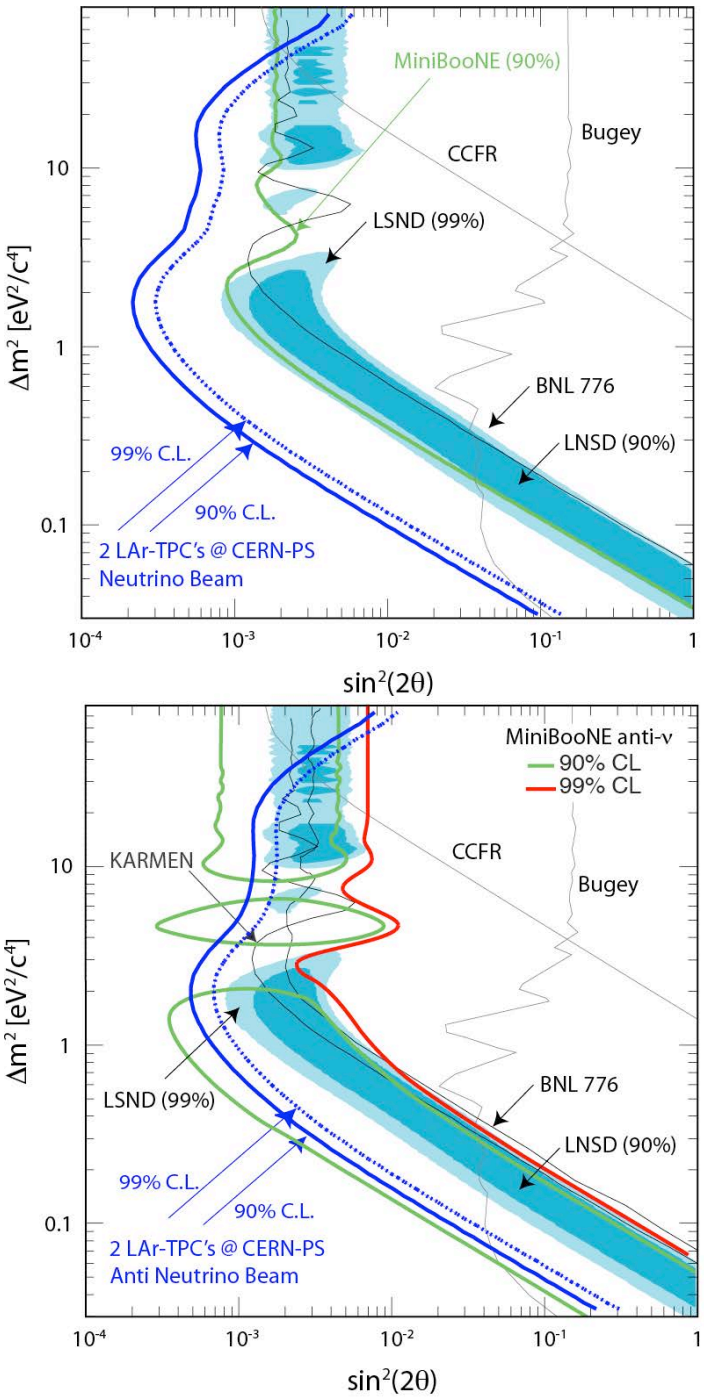

Figure 41. Expected sensitivity for the proposed experiment exposed at the CERN-PS neutrino beam (top) and anti-neutrino (bottom) for 2.5 10^{20} pot and 5.0 10^{20} pot respectively. The LSND allowed region is fully explored in both cases.

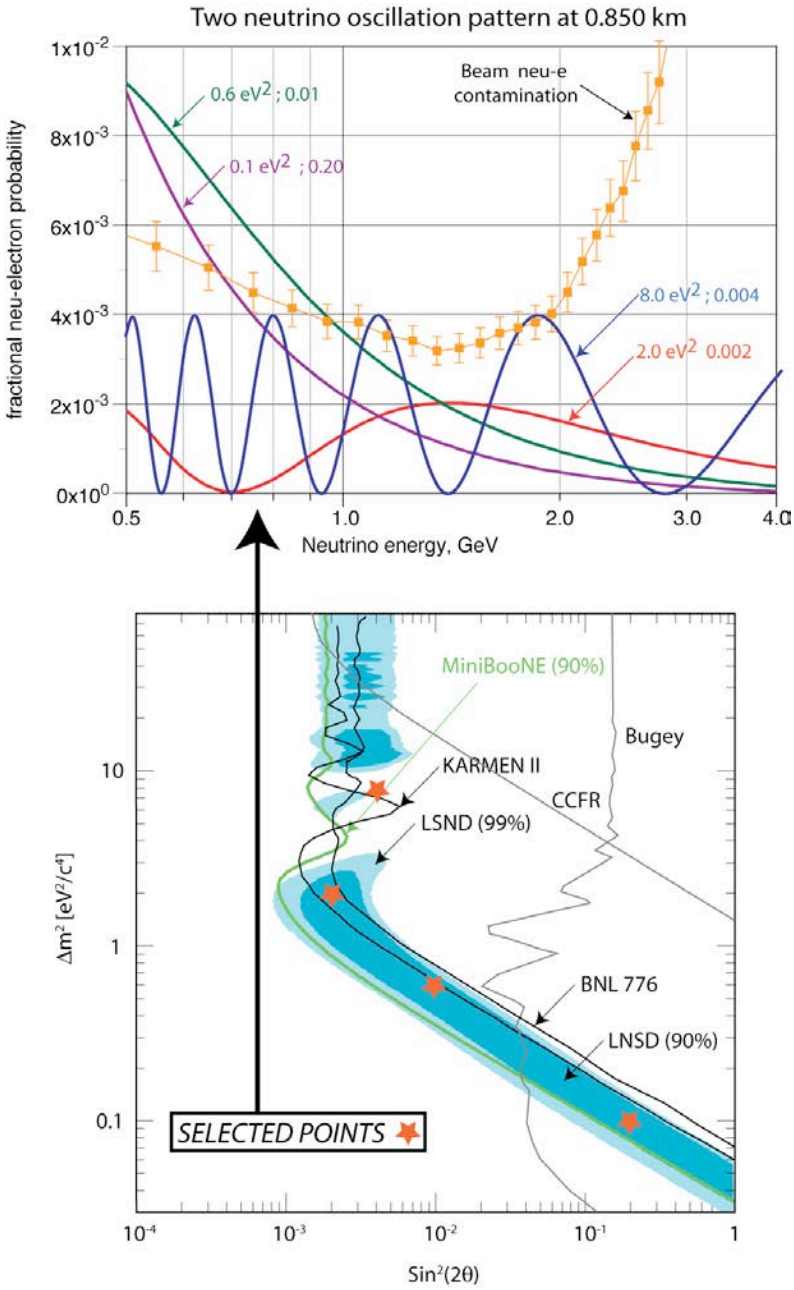

Figure 42. The experimentally expected oscillation patterns at 850 m shown for two neutrino oscillations and for some indicative positions of the LNSD allowed region (indicated with a star mark). The expected background due to the νμ beam contamination is also indicated.

5 Other physics issues

The large amount of data recorded by the proposed experiment will allow performing interesting measurements. The possibility of a combined search with NESSIE magnetic spectrometer [36] for the sign of the outgoing muons has to be mentioned. Neutrino cross-sections in the low energy region will be of interest for the forthcoming long base-line neutrino oscillation projects. Another topic covered by the experiment will be the search for neutrino radiative decay.

5.1 Neutrino cross-section measurements

The measure of neutrino cross section at low energy (E_ν ~ 0-2 GeV) is an argument of interest by itself and also for the modelling of signal processes and studies of background rejection in atmospheric and accelerator based neutrino oscillation experiments. Figure 25 shows a compilation of previous measurements of charged current neutrino interactions.

At these energies the dominant processes are quasi-elastic (QE) or single pion production processes, which have not been as well studied as deep inelastic scattering (DIS) reactions, which dominate at higher energies.

The present proposal, using a detector with very low detection threshold (tens of MeV), may improve significantly our knowledge in the interesting region (0 - 2 GeV).

The quasi-elastic process $\nu_\mu p \rightarrow \mu^- n$ peaks at ~ 0.5 GeV and dominates the total charged-current cross section for $E_\nu < 1$ Gev. This process has been studied mostly with low energy (100 MeV - 10 GeV) bubble chamber experiments on light targets more than 20 years ago. These experiments are plagued by low statistics (~ 10^3 events per experiment) and high systematic errors. As an example, flux uncertainty amounts to 15-20 %. New experiments, such as MiniBooNE, have recently produced new results on this subject [37], but the region around and below 500 MeV (of interest for Cherenkov detectors, such as T2K, for the accurate reconstruction of neutrino energies) may be measured precisely only with LAr-TPC detectors with very low thresholds.

Cross section theoretical calculations for free nucleons and aside nuclear effects have a theoretical uncertainty dominated by the effective axial mass M_A that enters in the axial form factor $F_A(q^2)$ [38]. The world average $M_A = 1.026 \pm 0.021$ GeV slightly disagrees with recent results from K2K [39]: 1.20 ± 0.12 GeV and MiniBooNE [40]: 1.25 ± 0.12 GeV and further investigations may be valuable.

Single pion CC production begins to dominate the cross section channels at E_ν ~ 1 - 2 GeV and some measurements are available from K2K, MiniBooNE [41] and Minerva. CC π^+ production is a crucial channel for ν_μ disappearance measurements (it can bias CC QE signal if the pion is lost), while NC single π^0 production is a relevant background for ν_e appearance analysis.

NC processes, such as NC π^0 production, are poorly measured in the region around 1-2 GeV. Available data are mainly from old bubble chamber experiments [36], with a new result from MiniBooNE [42] and a recent measurement from K2K [43] of $\sigma(\text{NC } \pi^0) / \sigma(\text{CC}) = 0.064 \pm 0.07$ at ~ 1.5 GeV. For oscillation searches, a measure of NC π^0 cross section would be valuable.

Table 4 summarises the expected number of events reconstructed in the proposed near detector at PS for a two year running period (2.5 x 10^{20} pot) for the main cross sections of interest. An increase of an order of magnitude in statistics is expected in some channels, as compared to published data.

Table 4. Expected number of events at the "Near" detector for 2.5 10^{20} pot for different reaction channels and energy ranges.

process	Energy region	statistics
ν_μ QE CC	< 1 GeV	1.9 x 10^6
ν_μ QE CC	1-2 GeV	1.9 x 10^6
ν_μ CC single pion	1-2 GeV	9.5 x 10^5
ν NC π^0	1-2 GeV	1.1 x 10^5

5.2 Search for anomalous single-photon excess events

As already mentioned, there are additional interpretations of excess events observed by LSND and MiniBooNe based on new physics processes with a single photon in the final state that can be tested with the PS experiment. Depending on the model, two signatures of the anomalous single γ's could be considered in the far detector:

A) presence of only a single γ produced due to anomaly-mediated neutrino-photon coupling in the reaction $\nu N \to \nu N \gamma$ [14]. The photon is emitted from the primary vertex at a small angle with respect to the neutrino beam;

B) presence of two separated clusters. The first one originates from the primary NC interaction producing the heavy neutrino ν_h, and another one from a converted γ emitted in the $\nu_h \to \nu\gamma$ decay in flight. It is assumed that the ν_h is produced through the mixing with the muon neutrino, and decays promptly, e.g. due to the transition magnetic moment μ_{tr} between the ν_h and the lighter ν state [15, 16].

In the case of scenario A, the search is based on the comparison of the observed and expected single-γ event rate in the far detector. The expected γ-

rate is found to be very low, and it will be cross-checked with a data-driven analysis of conventional reactions with a significant electromagnetic component in the final state, e.g. such as the coherent π^0 production, etc...

In the case of scenario B, the ν_h is assumed to be a relatively long-lived particle, which being produced, would penetrate the far detector without attenuation, and would be observed through its $\nu_h \to \nu\gamma$ decay followed by the decay photon conversion in the downstream part of the detector [16]. The experimental signature of the ν_h decay is the appearance of a single converted photon displaced from the primary vertex at a distance $\Delta l \gg \lambda$ (here λ is the effective interaction length of the detector) as schematically illustrated in Figure 43. Such a kind of a search has never been done before.

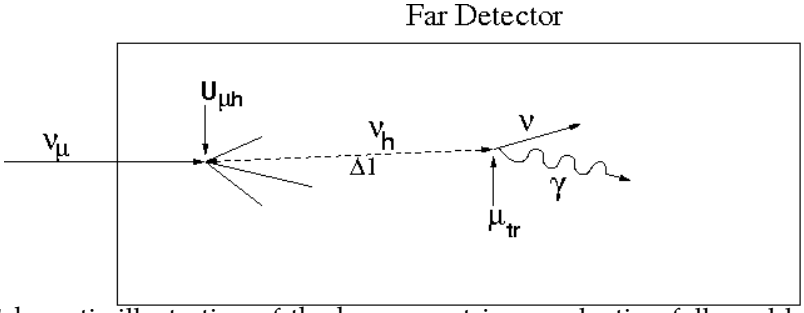

Figure 43. Schematic illustration of the heavy neutrino production followed by its prompt radiative decay in the far detector.

6 Time schedule for installation

The time schedule for the installation of the experiment at the CERN-PS is briefly discussed. In order to minimize the implications for the dismantling of the detector in the LNGS, we assume that for T600 option 2 is chosen. The internal detector will be extracted fully assembled from cryostats, with an existing, appropriate tooling and introduced in a container and an appropriate clean room will protect and support wire chambers and will be used as interface during transport. This solution permits to avoid major heavy works in Laboratory. In this option, the new cryostats should be built at CERN following the same design of the cryostat of the near detector and the same will be done for the external thermal screen. The main milestones for the T600 will therefore be the following:

- January – July 2012: design, call for tenders, order of the new cryostat and thermal screen;
- January – June 2013: site preparation of building 191 CERN (technical infrastructures and basement);
- September 2013: delivery of new cryostats and lateral walls of thermal screen installation, excluding one end cup in each cryostat to allow the TPC wire system introduction;
- November 2013: end of data-taking of ICARUS T600 at LNGS, empting, detector and cryogenic plant disassembling, Clean Room preparation at CERN Hall B-191;
- January – February 2014: transport of TPC structure from LNGS to CERN and installation, PMT system upgrade;
- March – May 2014: completion of thermal screen, erection of mechanical supports, cryogenic plant installation, cabling, electronics read-out and DAQ installation;
- June – July 2014: T600 test leak and DAQ;
- August 2014: LAr filling;
- September – October 2014: T600 final test and commissioning.

The main milestones for the T150 will be the following:

- January – July 2012: design, call for tenders, order of the new cryostat, thermal screen and inner TPC detector;
- January – December 2013: erection of the building for the near detector, including technical infrastructures and basement;
- September 2013: delivery of new T150 cryostat and installation of the thermal screens of the lateral walls;
- October – December 2013: clean-room preparation Inner detector installation, including TPC wire chambers, cathode, race–track and PMT;

- January – May 2014: completion of thermal screen, erection of mechanical supports, cryogenic plant installation, cabling, electronics read-out and DAQ installation;
- June – July: T150 test leak and DAQ;
- August 2014: LAr filling;
- September – October 2014: T150 final test and commissioning.

7 Acknowledgements

The Collaboration warmly thanks all the colleagues from the CERN BE, TE and EN Departments, whose suggestions, information and opinions have been essential to define the parts of this proposal concerning the transport of T600 from the Gran Sasso Laboratories and its installation at CERN.

We acknowledge not only the results, but also the collaborative and proactive attitude of the CERN working group in charge of the preliminary studies about the refurbishing of the PS neutrino facility.

8 References

[1] K. Nakamura et al., (Particle Data Group), J. Phys. G 37, 075021 (2010).

[2] B. Pontecorvo, Zh. Eksp. Teor. Fiz. 53, 1717 (1967) [Sov. Phys. JETP 26, 984 (1968)].

[3] G. Mention et al. arXiv:1101.2755v1 [hep-ex] and previous references therein.

[4] J. N. Abdurashitov et al. (SAGE Collaboration), Phys. Rev. C 80, 015807 (2009).

J. N. Abdurashitov et al. (SAGE Collaboration), Phys. Rev. Lett. 77, 4708 (1996).

J. N. Abdurashitov et al. (SAGE Collaboration), Phys. Rev. C 59, 2246 (1999).

J. N. Abdurashitov et al., Phys. Rev. C 73, 045805 (2006).

[5] F. Kaether, W. Hampel, G. Heusser, J. Kiko, and T. Kirsten, Phys. Lett. B 685, 47 (2010).

P. Anselmann et al. (GALLEX Collaboration), Phys. Lett. B 342, 440 (1995).

W. Hampel et al. (GALLEX Collaboration), Phys. Lett. B 420, 114 (1998).

[6] A. Aguilar et al. (LSND Collaboration), Phys. Rev. D 64, 112007 (2001).

[7] A. A. Aguilar-Arevalo (MiniBooNE Collaboration), Phys. Rev. Lett. 102, 101802 (2009).

A. A. Aguilar-Arevalo et al. (MiniBooNE Collaboration), arXiv:1007.1150.

[8] F.Mills, ICHEP 2010, Paris, France.

R. Van de Water, Neutrino 2010, Athens, Greece.
E.D. Zimmerman, PANIC 2011, Cambridge, U.S.A.

[9] C. Giunti, M. Laveder, Phys. Rev. D82 (2010) 053005 and previous references therein.

[10] E. Komatsu et al., arxiv.org/abs/1001.4538.

J. Dunkley et al., arxiv.org/abs/1009.0866.

J. Hamann et al. , arxiv.org/abs/1006.5276.

Y. I. Izotov, T. X. Thuan, arxiv.org/abs/1001.4440.

[11] C. Rubbia, CERN-EP/77-08 (1977).

A.Guglielmi, Neutrino 2010, Athens, Greece.

C. Rubbia et al., JINST 6 P07011 (2011).

[12] B. Baibussinov et al., arXiv:0909.0355v3;
ICARUS/CNGS2-P323 Collaboration, Physics Programme for ICARUS after 2012, SPSC-M-773 (2011).

[13] J. N. Bahcall, Phys. Rev. C 56, 3391 (1997).

[14] J. A. Harvey, C. T. Hill and R. J. Hill, Phys. Rev. Lett. 99 (2007) 261601 [arXiv:0708.1281 [hep-ph]]; A. Harvey, C. T. Hill and R. J. Hill, Phys. Rev. D 77 (2008) 085017 [arXiv:0712.1230 [hep-th]]; R. J. Hill, Phys. Rev. D 81 (2010) 013008 [arXiv:0905.0291 [hep-ph]].

[15] S. N. Gninenko, Phys. Rev. Lett. 103(2009)241802 [arXiv:0902.3802 [hep-ph]].

[16] S. N. Gninenko, Phys. Rev. D 83 (2011) 015015 [arXiv:1009.5536 [hep-ph]].

[17] M. Baldo-Ceolin et al., CERN/PSCC/80-130, PSCC/P33, 30-10-1980; C. Angelini et al. [PS180 Coll.], Phys. Lett. B 179 (1986) 307.

[18] M. Guler et al., CERN-SPSC/99-26, SPSC/P311, 1999.

[19] Information on CERN-PS neutrino beam refurbishing project available at: http://info-psnf.web.cern.ch/info-PSNF/Presentations.

[20] E. Gschwendtner and S. Rende, CERN-ATS-2011-193, 2011

[21] M. Calviani et al., CERN-ATS-Note-2011-088 TECH, 2011

[22] A. Ferrari at al., CERN-AB-Note-2006-038, 2006.

[23] ICARUS Coll., ICARUS initial physics program, ICARUS-TM/2001-03 LNGS P28/01 LNGS-EXP 13/89 add.1/01; ICARUS Coll., Cloning of T600 modules to reach the design sensitive mass, ICARUS-TM/2001-08 LNGS-EXP 13/89 add.2/01.

[24] F. Arneodo et al., Phys. Rev. D 74 (2006) 112001.

[25] S. Amoruso et al., Nucl. Instrum. Meth. A523 (2004), 275; S. Amoruso et al., Nucl. Instrum. Meth. A516 (2004) 68.

[26] G. Charpak et al., Nucl. Instrum. and Meth. 80, (1970), 13.

[27] S. Amerio et al., Nucl. Instr. And Meth. A527 (2004) 329.

[28] P. Fessia et al., available at https://edms.cern.ch/document/1148527/1.

[29] Carpanese C. et al., IEEE Trans. on Nucl. Science. Vol. 45 no. 4 (1998), 1804;
Carpanese C. et al, Nucl. Instr. and Meth A409 (1998) 229;
Centro S. et al., Nucl. Instr. and Meth A412 (1998) 440.

[30] A. Ankowsky et al., Acta Phys. Pol. B 41 vol. 1 (2010) 103.

[31] A. Ankowski et al., Eur. Phys. J. C48 (2006) 667;
K. Cieslik et al., ICARUS-TM/07-02 (2007);
F. Varanini, HEP 2011, Grenoble, France.

[32] S. Amoruso et al., Eur. Phys. J. C33 (2004) 233.

[33] J. Altegoer et al., Nucl. Instr. And Meth. A404 (1998) 96; P. Astier et al., Nucl. Instr. And Meth. A515 (2003) 800; J. Altegoer et al., Nucl. Instr. And Meth. A428 (1999) 299.

[34] G. Battistoni et al., "The FLUKA code: Description and benchmarking", AIP Conf. Proc. 896, 31-49, (2007); G. Battistoni et al., A neutrino-nucleon interaction generator for the FLUKA Monte Carlo code, Proceedings of the 12th International conference on nuclear reaction mechanisms, Varenna (Italy), June 15 - 19, 2009, p.307; Ferrari et al., FLUKA, a multi particle transport code (program version 2005), CERN-2005-10, INFN/TC-05/11, 2005.

[35] G. Battistoni et al., Acta Phys. Polon. B37 (2006) 2361.

[36] P. Bernardini et al., CERN-SPSC-2011-030; SPSC-P-343, 2011.

[37] A.A. Aguilar-Averalo, Phys. ReV. D81 (2010) 092005.

[38] C.H. Llewellyn Smith, Phys. Rep. 3C (1972) 261.

[39] R.Gran et al., Phys. ReV. D74 (2006) 052002.

[40] T. Katori, talk Nuint07, Fermilab, May 2007.

[41] A.A. Aguilar-Averalo et al, Phys.ReV. D83 (2011) 052007.

[42] A.A.Aguilar-Averalo et al., Phys.ReV. D81 (2010) 013005.

[43] S. Nakayama et al., Phys. Lett. B619 (2005) 255.